RHEOLOGY AND CHARACTERIZATION OF HIGH-SOLIDS SUSPENSIONS FOR DIRECT INK WRITING OF ENERGETIC MATERIALS

A Dissertation
Presented to
The Academic Faculty

By

Hannah Kathryn Woods

In Partial Fulfillment
of the Requirements for the Degree
Master of Science in the
School of Materials Science and Engineering

Georgia Institute of Technology

August 2019

RHEOLOGY AND CHARACTERIZATION OF HIGH-SOLIDS SUSPENSIONS FOR DIRECT INK WRITING OF ENERGETIC MATERIALS

Approved by:

Dr. Blair Brettmann, Advisor
School of Chemical and Biomolecular Engineering
School of Materials Science and Engineering
Georgia Institute of Technology

Dr. Naresh Thadhani
School of Materials Science and Engineering
Georgia Institute of Technology

Dr. Mary Lynn Realff
School of Materials Science and Engineering
Georgia Institute of Technology

Date Approved: July 3, 2019

Dedicated to my dad and my grandpa Bill, the two most influential engineers in my life.

ACKNOWLEDGEMENTS

I would like to acknowledge my advisor Dr. Blair Brettmann and thesis committee members Dr. Naresh Thadhani and Dr. Mary Lynn Realff for their guidance, time, and effort in making this thesis possible. I want to acknowledge Andrew Boddorff for working with me on print method development, and for the good road trip conversations. Thank you to undergraduate researchers Zachary Adams, Mitchell Ketcham, and DJ Jang for your hard work and enthusiasm with rheology and printing experiments. Thanks to Didier Montaigne, Tammy Metroke, and Robert Barnes at the AFRL Munitions Directorate at Eglin Air Force Base for their project collaboration and for hosting us on multiple occasions. I also want to thank Karl and Davo at Hyrel 3D for their assistance with special printer setups and printing procedure development. Thank you to Manali Banerjee and Elena Ewaldz for SEM images, and to Elena Ewaldz for zero shear rheology measurements. I would also like to acknowledge Dr. Kimberly Kurtis and Xenia Wirth at Georgia Tech for generously allowing and showing me how to use the particle size analyzer.

Thank you to the Brettmann lab at Georgia Tech for a great lab experience, and especially thank you to my graduate labmates Elena Ewaldz, Nasreen Khan, and Manali Banerjee for their advice and encouragement. Thank you to my Georgia Tech family, especially Amy Brummer and Sven Voigt, for your ongoing emotional support. Special thanks to my therapist for both personal and academic guidance, and finally, thank you to all my friends and family for always being there for me.

TABLE OF CONTENTS

LIST OF TABLES

LIST OF FIGURES

LIST OF ABBREVIATIONS

AM	additive manufacturing
AMEM	additively manufactured energetic material
BisGMA	bisphenol A-glycidyl methacrylate
BP	boiling point [°C]
CAD	computer aided design
DAC	dual asymmetric centrifuge
DMF	dimethylformamide
DIW	direct ink writing
EtAc	ethyl acetate
FDM	fused deposition modeling
HTPB	hydroxyl terminated polybutadiene
IPDI	isophorone diisocyanate
LVR	linear viscoelastic regime
PBX	polymer bonded explosive
PDMS	polydimethylsiloxane
PIB	polyisobutylene
PMMA	polymethylmethacrylate
PET	pentaerythritol
PP	polypropylene

PVP	polyvinylpyrrolidone
RAM	resonant acoustic mixing
SEM	scanning electron microscopy
SLA	stereolithography
SLS	selective laser sintering
TEGDMA	triethylene glycol dimethacrylate
UV	ultraviolet
vol%	volume percent
VP	vapor pressure [Pa]
wt%	weight percent

LIST OF SYMBOLS

G’	storage modulus [Pa]
G”	loss modulus [Pa]
M_w	molecular weight [kDa = 1,000 g/mol]
$SrTiO_3$	strontium titanate
η_0	zero shear viscosity [Pa·s]
σ	shear stress [Pa]
$\dot{\gamma}$	shear rate [s^{-1}]

SUMMARY

Direct ink writing is a promising approach for preparing energetic materials with unique geometries that are of great interest in military and civil engineering fields due to their potential to control shock wave propagation and energy focus or dissipation. However, there are significant challenges to overcome in using additive manufacturing to produce energetics, particularly in using inks with high particle content (>60 vol% particles) while maintaining both extrusion capability and print quality. Voids and interfaces in energetics are areas of high risk for hot spot formation, and with the layer-by-layer additive manufacturing process, voids can manifest both between and within the extruded filaments as well as between printed layers. Concerns associated with the challenges of printing high-solids suspensions make understanding the flow and print capabilities of these materials of great importance.

The binder used in suspensions for direct ink writing plays an important role in overall flow characteristics of the ink, and therefore has significant impact on final print quality. In this work, glass microspheres in polymer-solvent and photocurable monomer binders are examined as model systems to provide an in-depth study of polymer binder design. This work aims to understand how binder characteristics affect the viscosity and printability of such high-solids suspensions. We show that the suspension viscosity is primarily controlled by the particle volume fraction for the photocurable binder system, while both the particle volume fraction and polymer molecular weight influence the viscosity in the case of the polymer-solvent binder system. Both binder types can be tuned to make printable suspensions that result in lines of consistent width and 3D disc-shaped objects, indicating that both paths show promise for future direct ink writing formulations of energetic materials.

CHAPTER 1
INTRODUCTION

Since its debut in the 1980s [1], additive manufacturing (AM) has been a transformative innovation in countless industries for rapid prototyping and producing custom parts, including applications such as medical implants and prosthetics [2, 3], tissue engineering [4], dental restoratives [5, 6, 7], aerospace parts [3, 8], and the automotive industry [9]. Fused deposition modeling (FDM), stereolithography (SLA), and selective laser sintering (SLS) are three of many currently well-developed and widely used technologies. In the FDM process, a thermoplastic filament is melted and deposited layer by layer and solidifies upon cooling to produce a 3D part [10]. In SLA, a container of light-sensitive liquid resin is irradiated in specific patterns at select wavelengths to crosslink and harden the resin in the shape of the programmed 3D part [11]. The SLS process utilizes a laser to melt or sinter together powder (can be metallic, plastic, ceramic, or any fusible powder) layer by layer to form a 3D part [12, 13, 14].

One of the most flexible methods of AM is direct ink writing (DIW), which will be discussed in greater detail in this chapter, a process that allows for the use of highly custom inks tailored to specific applications [15]. DIW provides a unique opportunity to fabricate energetic materials in geometries that are traditionally difficult or impossible to manufacture via subtractive means, in particular engineered lattice and cellular structures for wave focusing or energy dissipation [16]. This goal of this work is to understand the influence of binder properties on the viscosity and printability of custom high-solids suspensions for DIW of energetic materials, focusing on the polymer binder used in an energetic materials system.

1.1 The Direct Ink Writing Process

Direct ink writing (DIW), also known as robocasting, is a form of additive manufacturing in which a paste-like ink in a syringe is extruded through a nozzle to vertically build up 2D layers one after another to produce a 3D geometry. Figure 1.1 shows an illustration of the direct ink writing process, with labels showing the syringe filled with paste-like ink that is extruded through the nozzle onto the build platform. The first and third 2D layers are also labeled to show the order in which layers are built upon one another. The print pattern can be achieved through either movement of the print head and nozzle itself, or through translation of the build platform, depending on the technology [17, 18].

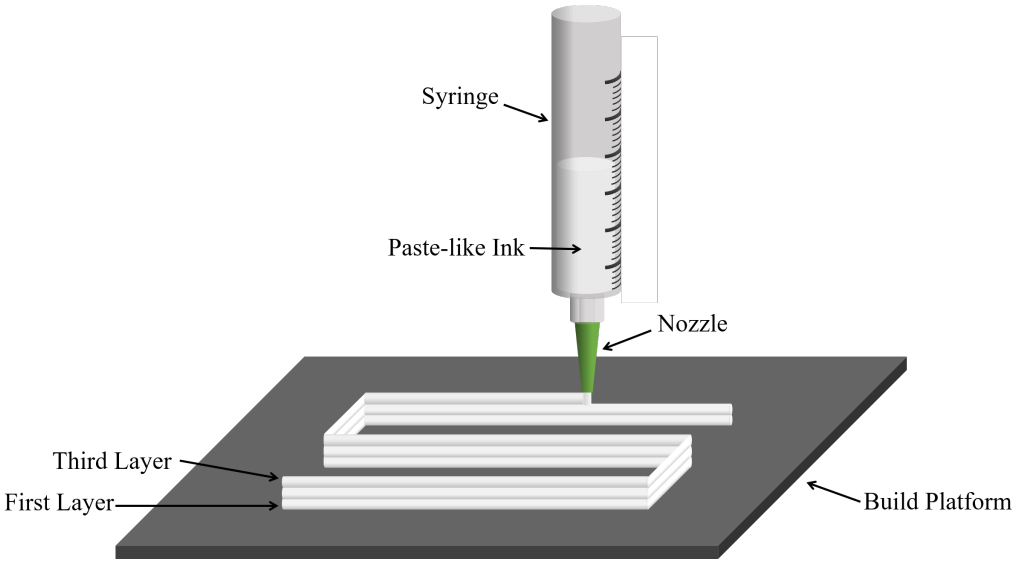

Figure 1.1: Illustration of the direct ink writing dispensing set-up.

Successful printing via DIW involves using an ink with predictable and well-understood viscoelastic properties and optimizing printer settings to accommodate those properties. The viscosity of the ink should be balanced such that it is low enough to not require excessive pressure buildup to overcome the yield stresses necessary to induce flow through the nozzle, but be high enough to maintain its structure post-extrusion [18, 19]. This is why shear-thinning materials are particularly favored in DIW applications. Maintaining rigidity

post-extrusion in bottom layers becomes more and more important as subsequent layers are built, as the bottom layers must be able to support those that are built on top.

Key printing parameters include material extrusion or flow rate (how quickly material flows out of the syringe), print head speed (how quickly the nozzle moves in the level 2D plane), and layer height (how far up the nozzle moves to begin printing the subsequent 2D plane on top of the previous). In addition, many printers allow for control of the build platform temperature and the material this is made of (glass, painter's tape, transparencies) including whether or not a primer is used, which can have significant impact on material adhesion to the build platform. The primary properties besides suspension composition that need to be considered for DIW are sorted into physical and software-controlled parameters in Table 1.1.

Table 1.1: Table of primary tunable properties of direct ink writing.

Physical Parameters	Software-Controlled Parameters
Nozzle Diameter	Print Speed
Nozzle Shape	Flow Rate
Syringe Size	Layer Height
Build Platform Material/Primer	Bed Temperature

The ability to tune so many parameters makes DIW an exceptionally adaptable process, capable of using versatile inks, but this also makes it challenging to balance all these variables when working with a newly designed custom ink. If a suspension has too low of a viscosity, material may leak from the syringe even without applied pressure to the plunger, or more material than desired could come out upon applied pressure leading to over-extrusion. Conversely, under-extrusion can also take place if the suspension has too high of a viscosity and the plunger cannot apply sufficient pressure to initiate material flow. Additionally, the print head speed needs to be balanced with the flow rate so that the suspension does not dispense more than necessary for each layer (similar results to over-extrusion) caus-

ing imprecise and collapsed prints where the nozzle unnecessarily drags excess material along with it, or so that it isn't spread too thin (similar results to under-extrusion) causing a void-filled product. Depending on the application, these parameters can be tuned to accommodate printing of varying structures, including lattice structures that must maintain shape despite gaps in previous layers [17].

The viscosity of a material is a key factor in its printability, particularly with regards to determining optimal printer settings for extrusion (to avoid both under- and over- extrusion) and desired printed parts [20]. Because high-solids suspensions tend to have a very high viscosity [21], it is difficult to produce consistent flow, particularly for starting and stopping material extrusion. Even once steady-state flow is reached, it is possible that the print head speed will need to move slower to accommodate a slower material extrusion rate that could be associated with the highly viscous ink, decreasing production efficiency.

A significant proportion of current application areas for DIW are in ceramics because of the slurry-suspension nature of those materials and the difficulty in using other methods (such as aforementioned FDM, SLA, or SLS) with such materials. Similarly, DIW was selected for this energetic materials application due to its ability to accommodate highly customized inks that would otherwise be impractical with other methods.

1.1.1 Considerations of Printing with High-Solids Suspensions

In DIW additive manufacturing, inks are generally composed of particles suspended in a liquid binder. In the case of high-solids suspensions, these inks are comparable to a very dense paste. High-solids suspensions find their definition at the crossover from highly filled colloidal dispersions to granular materials. Colloidal dispersions are comprised of insoluble particles suspended in a continuous phase [22]. On the other end of the spectrum, wet granular materials are also comprised of insoluble particles in a matrix but differ from colloidal suspensions because they do not have enough binding material to completely fill the interstitial space between particles and thus tend to form liquid bridges between particles

[23, 20]. This bridge is a characteristic of weakly wetted inks with such high solid loading that they are not completely surrounded by the binder matrix. Wet granular materials are used in production of some pharmaceutical products, but these typically require compression to give them strength [24]. High-solids suspensions generally have higher particle content than colloidal dispersions yet not quite enough particle content to be considered a wet granular material. Here we discuss important aspects of materials that fall into these categories.

1.1.2 Particle Properties Affecting Printability

Individual particle characteristics also play an important role in the printability of high-solids suspensions, and much research has gone into understanding the role of particle size, shape, aspect ratio, modality, size distribution, and surface chemistry [25, 20, 26, 21]. Some key highlights from these studies are presented in this section.

Particle Shape

The aspect ratio is defined as the length of particle divided by the diameter (L/D). As the aspect ratio of particles increases, so does the relative viscosity for any given volume fraction of those particles [26]. For example, spherical particles of the same composition as rod-like particles will exhibit a lower viscosity than their rod-like counterparts at the same volume fraction and at the same conditions.

Particle Size

Work done by Sweeney et al. [20] explored 3D-printing of wet granular material with particles on the microscale (10s to 100s of μm) using rheology and extrusion tests with a mixture of pentaerythritol (PET) particles and polydimethylsiloxane (PDMS, a silicone-based binder). They studied particles with 3 different size ranges, 38-75 μm, 75-90 μm and 230-350 μm, in order to understand how particle size influences rheology. Their tests

all used 20% mass percent of PDMS and 80% mass percent of particles. All materials in that study displayed shear-thinning behavior and the consistency of the mixtures reportedly ranged from silly putty (38-75 μm), to wet sand (75-90 μm), to coarse grains loosely held together (230-350 μm). Viscosity was highest for the smallest particles due to interparticle friction because of the larger surface area present in the smaller particle mixture. Similar results have been obtained by other research studies [25, 27, 28] showing that, in general, smaller particle sizes will lead to higher viscosities and therefore require greater pressure to induce flow through a print nozzle.

Maximum Packing Fraction and Particle Modality

The total volume percent (vol%) that particles take up within the ink can significantly affect viscous properties of solutions and suspensions [29, 30]. Maximum packing fraction refers to the volume fraction of space filled by particles packed as closely as possible in an arbitrary total volume where the continuous phase is air. For highly ordered hexagonal packing of monodisperse hard spheres (spheres of all the same size), the maximum packing fraction is 0.74 but for random packing of monodisperse hard spheres, the maximum packing fraction is only 0.64 [29, 30]. These are the maximum packing fractions for spheres, regardless of sphere size.

The concept of using mixtures of particle sizes (bimodal distributions, trimodal, etc.) can also be used to tune the suspension viscosity [31, 32]. Using different particle modalities can increase the maximum packing fraction [33]. In the bi- and multi- modal systems, smaller particles can fill interstitial sites of larger particles to allow for even higher particle packing fractions [21, 31]. An illustration highlighting these effects is shown in Figure 1.2.

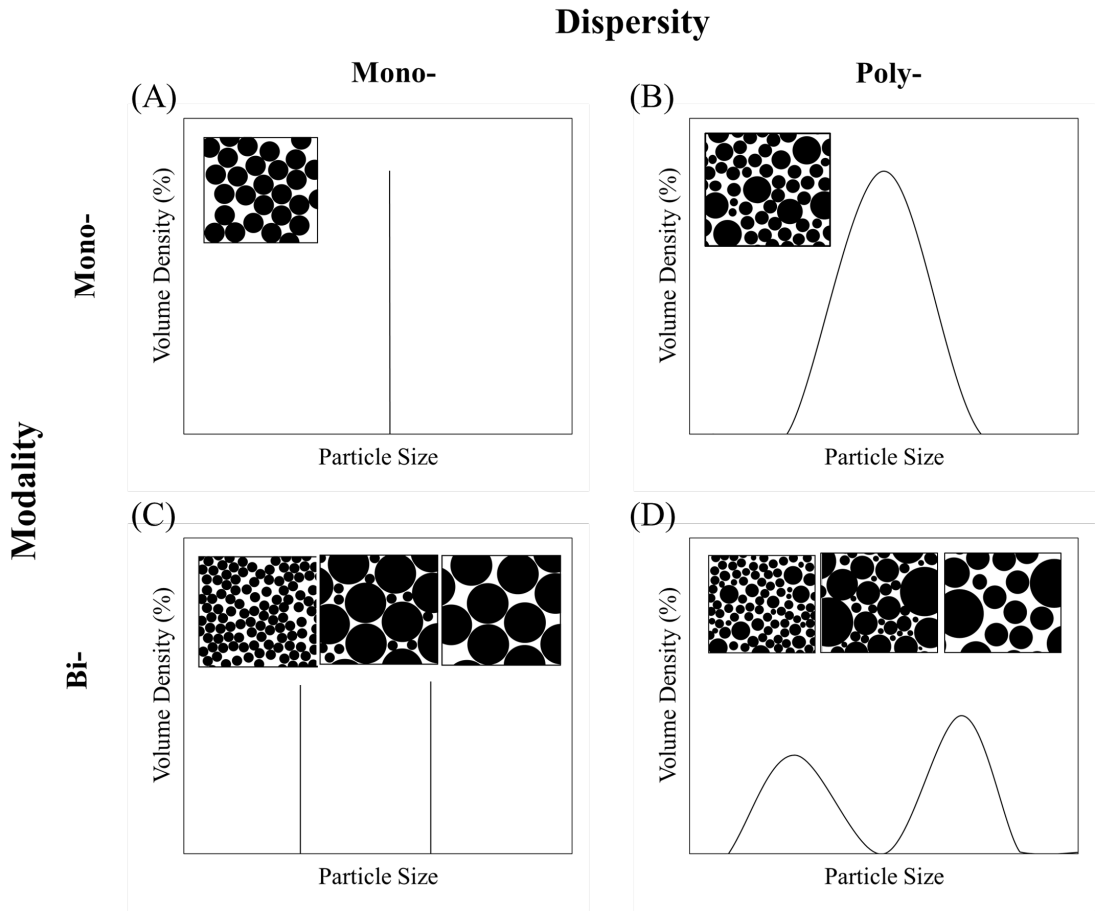

Figure 1.2: Illustration showing the difference between particle size distribution and modality for (A) a monomodal monodisperse system, (B) a monomodal polydisperse system, (C) a bimodal system comprised of two monodisperse systems, and (D) a bimodal system comprised of two polydisperse systems.

Particle Dispersion and Agglomeration

Poor particle dispersion (not to be confused with dispersity) and particle agglomeration can pose a challenge when dealing with high-solids suspensions. If the particles cannot maintain buoyancy in the suspension, a gradient through the syringe can form, causing earlier print layers to contain higher percentages of particles than subsequent layers. Adequate mixing of suspensions can help to minimize print issues associated with this. Additionally, if the particle size is on or near the same order of magnitude as the diameter of the nozzle

opening, this can cause particles to pack in and clog the nozzle, stopping extrusion [34]. This phenomena should not be confused with what is referred to as jamming, discussed in the next section.

The Jamming Transition

The jamming transition for granular materials and dense colloidal suspensions is associated with the approach of the maximum or critical packing fraction [35], but refers to the confined state in which direct contact between particles forms a stress-supporting network (also called force chains) that causes shearing to stop entirely [36, 37, 38]. In other words, jamming occurs once the particles are no longer in a flowable state and behave like a solid, but this does not necessarily require the suspension to be at its critical packing fraction because not all particles need to be involved for a load-bearing network to form [39]. Jamming has mostly been studied in the context of dry granular materials in confined environments (with boundary conditions) [35, 37]. More recent developments in this area have led to a distinction of shear-jammed states at volume fractions below the critical packing fraction and isotropically jammed states [40].

1.2 Additive Manufacturing of Energetic Materials

In the development of energetic materials, there is great interest in novel geometries, such as lattice structures and gradient materials, as they have the potential to allow better control over shock wave propagation and energy dissipation [16]. Shaped charges are used commonly in civil engineering applications [41], and using AM to fabricate revolutionize their production. Traditional fabrication processes for energetic materials include casting and rolling [42, 43], but achieving novel geometries with these methods is limited. Subtractive means for manufacturing such unique shapes such as lattice structures for energetics would be both impractical and wasteful. A few other advantages that AM has over traditional manufacturing methods include decreased material cost and the potential to build on-demand

structures to minimize safety and space issues in storing energetic parts. However, there are a number of challenges to overcome to make additively manufactured energetic materials (AMEMs) a reality.

Predictability and strict control of energetic materials is vital to their safety and functionality, which requires a standardized and highly controlled manufacturing method. Some challenges in the feasibility of the AM processing of energetic materials include voids, hot spots, and intra- and inter- layer defects, all of which can cause instability. Hot spots are energy-localized ignition points in energetic materials with many causes including jetting of the binder to fill a void space, void collapse, and heating of trapped gas [44, 45, 46]. Typical locations for hot spot formation are points of transgranular fracture or the interface where the polymer binder may delaminate from the energetic particles, but hot spots can occur at voids formed by other means as well [47]. Excessive heating in energetics due to friction or hot spots in these materials can give rise to unwanted and untimely detonation, making this an important consideration for any new materials or processes.

With regards to AMEMs, potential sources of voids are much higher than they would be in a similar system made via traditional manufacturing (casting or rolling) due to the layer structure and the flow-based processing. These voids can exist on multiple length scales and appear in between or within the extruded filaments. Inter-layer voids are prevented by aiming for 100% infill, but one particular aim in current AMEM research is to determine when the scale and distribution of the voids ceases to influence the shock properties, which could provide more tolerance to gaps forming between filaments.

1.2.1 Binder Selection for Energetics

Common binder systems in energetic formulations of polymer bonded explosives (PBX) include hydroxyl terminated polybutadiene (HTPB), estane, polyisobutylene (PIB), polymethylmethacrylate (PMMA), polydimethylsiloxane (PDMS) and other polyurethane-based polymers [47, 48, 49, 50, 51]. Selection considerations for energetic binders include den-

sity, degree of crosslinking, elasticity, and mechanical properties. A key factor to prevent undesired detonation and maintaining a safe-to-handle final product for PBX is the shock absorbency of the binder. The goal of the binder is to house the energetic particle in a stable, less vulnerable environment that is resistant to undesired detonation, until it is ready to be detonated. Daniel [48] studied polyurethane PBX systems as a good shock absorbent option for cast systems of formulations with 84% and 88% particle loading content with a HTPB and (isophorone diisocyanate) IPDI-based binder.

1.2.2 Prior Work on DIW Energetic Simulants

The use of simulant materials for energetic formulation research aims to provide a safe, cost-effective way to study these systems. Such simulants that are chosen to match key density, stability, and solubility properties have previously included sugar crystals, acetaminophen, and PET [52, 53, 20]. Research studies on parts made with inert formulations have been done to show the similarities of fracture behavior between live materials and such simulants [54, 55].

Limited studies have been done using the previously discussed binders and surrogate particles for actual DIW, at least that have been published publicly and are available to us. A study done by Ruz-Nuglo et al. [52] explored direct writing techniques for mock energetic materials up to 94 wt% solid loading. They used strontium titanate ($SrTiO_3$) with 5 μm mean particle size, and tried a second mock material as a mixture of powdered and granulated pure cane sugar, and with a silicone Sylgard polymer matrix. They found that the Sylgard-$SrTiO_3$ mix printed much more smoothly than the Sylgard-cane sugar mixture. They attributed this difference to the irregular particle morphology and large sugar particles causing poor printing results. These results indicated that the PBX behaves similarly to other high-solids suspensions, but the studies do not thoroughly investigate the effects of binder properties, such as molecular weight and binder viscosity, on the rheology of the suspension.

The previously described work by Sweeney et al. ([20], Section 1.1.2) used PET particulates as intended energetic simulants due to their similarities to metallic colloids found in energetic materials. They examined the print quality of formulations with three particle size ranges and how the print quality correlated to the rheological properties. Their work with the 38-75 μm particle size range (with the highest viscosity of the three primary systems they worked with) showed a significant decrease in print quality with increasing applied pressure (from 60 to 80 PSI). They found through their preliminary studies that, while it is challenging to generate high quality with such highly viscous inks, there is still promise in continuing research and work with highly loaded suspensions for energetic applications.

1.3 Motivation

Development of AMEM technology is of great interest in military and civil engineering fields due to the potential to control shock wave propagation and energy dissipation via novel geometries. The goal of this work is to demonstrate the potential for DIW of energetic materials through examination of rheology and print flow properties of an inert simulant in two different binder systems. We aim to develop a method for printing AMEM simulants in a cost-effective, safe, and easily reproducible manner. This work serves as a framework for understanding the role of binder type and properties in high-solids suspensions, with a particular application in AMEMs.

1.4 Thesis Objectives

Objective 1:

Characterize and understand the implications of individual suspension components, in particular binder properties, on suspension rheology. (Addressed in chapter 2)

Objective 2:

Determine viscoelastic properties of particle-binder suspensions for varied solid particle content of glass microspheres in polymer-solvent and photocurable binder systems. (Addressed in chapter 3)

Objective 3:

Demonstrate printability of both the polymer-solvent and photocurable systems and relate to viscoelastic properties determined in Objective 2, and assess print quality. (Addressed in chapters 3-4)

CHAPTER 2
MATERIAL SELECTION AND CHARACTERIZATION

2.1 Background

As stated in chapter 1, DIW inks are often composed of solid particles suspended in a binder and post-processing is typically required after printing to solidify the binder and make the part usable. Understanding the mechanisms behind these solidification processes and understanding what properties can be used to tune the binder viscosity can save time and energy when creating new suspension formulations and developing consistently high quality prints. Even without changing the solid filler material, altering the binder properties can have a significant impact on viscosity and printability [51]. The work described in this chapter focus on the selection of materials that will aid in assessing the viscoelastic properties of high-solids suspensions for DIW.

2.1.1 Binders for DIW Suspensions

Two common methods of solidifying high-solids suspensions post-printing are solvent evaporation and polymerization, shown in Figure 2.1. The end goal of both methods is the same: to attain the solid energetic particulate bound together in a polymer matrix as a composite solid (hence the phrase polymer-bonded explosives PBXs [51]). But there is a major difference between these two methods: the starting constituents. In the solvent evaporation method the starting constituents are a polymer dissolved in a solvent in which the energetic particles are dispersed. In contrast, the polymerization starting constituents are monomers and an initiator in which the energetic particles are dispersed, requiring a trigger mechanism to initiate solidification. These processes, along with rationale behind the materials chosen for experiments, are examined in more detail in this chapter.

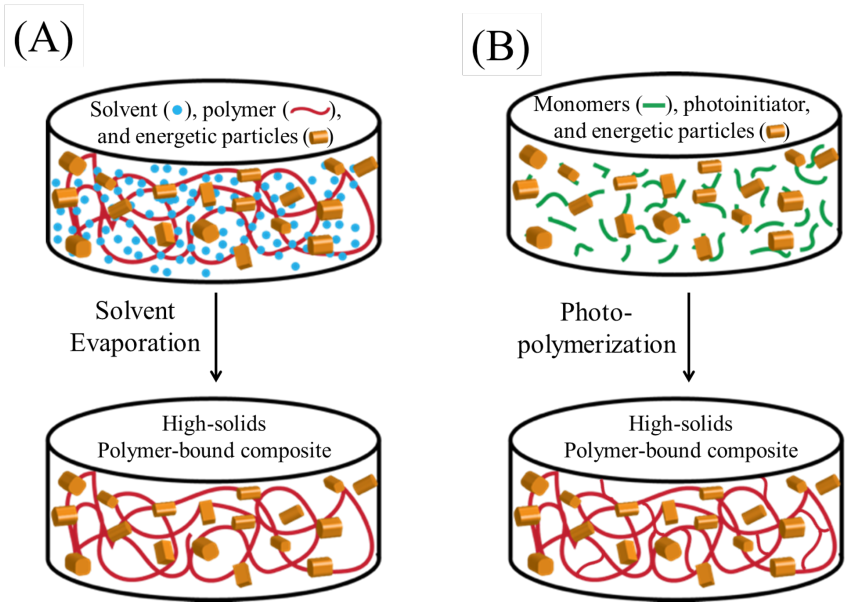

Figure 2.1: Illustration of (A) the solvent evaporation process and (B) the photopolymerization solidification process for formation of polymer bound composites from high-solids suspensions.

2.1.2 Solvent Evaporation Binders

For the polymer-solvent binder method, (Figure 2.1A), the binder is essentially a high viscosity polymer solution [56]. After the solvent evaporates, the polymer remains as the cohesive component holding all the particles together. In polymer solutions, a higher molecular weight leads to higher viscosities [57], and this relationship can be used to our benefit to tune the viscosity of the binder solutions through variations in molecular weight.

The primary consideration when working with these solvent-based binders is the volatility of the solvent. The evaporation rate must be tailored to have a balance between a reasonable rate of solidification to minimize print time, but not such a fast rate that the ink dries out too quickly during syringe loading or that the nozzle clogs during printing. Work done by Jakus et al. [58] showed that metal and metal-oxide powders suspended in a an elastomer and tri-solvent binder system produced shear-thinning inks capable of free-form AM extrusion, aided by rapid dichloromethane (DCM) evaporation (vapor pres-

sure (VP)=57.3 kPa, boiling point (BP)=39.6°C). However, the remaining low-volatility components in the tri-solvent system were left behind and the printed structures required post-processing to remove these solvents and sinter the green bodies. The need for post-processing is very common in AM of ceramics [14, 18, 58, 59], and the desire to avoid this differentiates the prior studies on ceramics from those involving AMEMs.

Jakus et al. [58] also reported nozzle clogging when the particle:polymer ratio exceeded 7:3 and went up to 8:2 and 9:1, but the solvent volume contents in their inks were not measured, so it is difficult to draw parallels to our system based on this. Rueschhoff et al. [18] varied the particle content for alumina/polyvinylpyrrolidone (PVP) aqueous suspensions from 51 to 58 vol% and demonstrated the ability to use DIW with a solvent evaporation approach for relatively highly loaded ceramic suspensions. Because of our desire to move to energetic applications for DIW and the importance of high loading to energetics, where 80-90 vol% loadings in the final product are preferred, the limits of these loadings with the solvent evaporation method were approached and tested.

2.1.3 Polymerizable Binders

The polymerization process (Figure 2.1B), begins with small molecule monomers and can be initiated by various stimuli including chemical catalysts, heat, or light [57]. In the context of energetic applications, the use of chemical catalysts or added heat for curing raises safety and stability concerns because of the possible temperature increase in such materials [60]. For this reason, photopolymerization (a type of free-radical polymerization initiated by light exposure [61]) is promising, as it requires only short exposure times in a fairly easily controllable environment. The work in thesis focuses on polymerization of a photocurable binder system that is initiated by ultraviolet (UV) exposure, minimizing unwanted premature curing under the visible light spectrum. One advantage of using photopolymerization-based solidification is that, unlike the solvent-based system, it does not use volatile compounds [62, 63, 64].

When using a photocurable binder for a high-solids suspension for DIW, important considerations include understanding the depth and speed of cure with respect to layer height and the effect of solid particulate and its refractive index on curing properties, as well as any shrinking or warpage caused by the polymerization process. Photocurable binder systems have also been used in AM of ceramics [59], but often still require much post processing to burn out the binder and sinter the remaining ceramic. Photocurable binder systems that do not require post-cure sintering are commonly used in dental composites to form a crosslinked polymer network [65, 66, 67]. Using photocurable binders for AMEMs will require a combination of the knowledge from ceramics AM and photopolymerization with the knowledge of the curing properties from dental composites.

A study by Cho et al. [68] investigated the effects of up to 20 wt% silica nanoparticles (7-40 nm) in a UV-curable acrylate monomer system and showed that addition of the nanoparticles actually increased monomer conversion rate up to 15 wt% (53% conversion in neat binder, 68% conversion for 15 wt% filler). They attributed this increase in part to the particles improving chain mobility. Monomer conversion slightly decreased upon increase of the filler to 20 wt% (64% conversion for 20 wt% filler) but studies with particles of such small sizes fall into the category of nano-fillers [69]. Use of much larger particles was examined by Gonçalves et al. [70] with barium glass particles (average size 2 μm) in a binder of bisphenol A-glycidyl methacrylate (BisGMA) and triethylene glycol dimethacrylate (TEGDMA). They showed that changing the inorganic content in 5 vol% increments from 25 to 60 vol% of these larger particles had no effect on degree of conversion. They attributed this lack of effect to the low surface area due to the large particles.

Shrinkage of the binder as it crosslinks and the associated induced stresses pose another challenge associated with using photocurable systems, with shrinkage percentages typically between 0.1 to 5% for photocurable systems and on the higher end of that for BisGMA:TEGDMA systems [65, 71, 70]. The aforementioned study by Gonçalves et al. [70] showed that volumetric shrinkage decreased from 3.3% to 2.1% when the particle content

increased from 25 to 60 vol%, associated with a decrease in polymerization stress from 5.8 to 3.9 MPa, respectively. In general, shrinkage has been shown to be reduced upon addition of fillers [67], so it may be only a minor consideration in this study. Despite inevitable shrinkage with these systems, just as UV curing between each DIW layer is advantageous in circumventing depth-of-cure limitations, the layer-by-layer process may also alleviate some of the concerns associated with warpage/cracking due to shrinking as curing occurs in successive layers and not in bulk. Atmospheric conditions can significantly affect curing, both the monomer conversion kinetics and the mechanical properties of the final product [68, 72], making control of the print environment an important factor in procuding reliable results.

2.2 Binder Development and Characterization Methods

2.2.1 Solvent-based System

To design a solvent-based system for DIW with high-solids suspensions, the primary goal was to achieve moderate solvent volatility, where the drying time was not excessively long but also not too short so that the material stream did not dry in the nozzle. A variety of initial systems were examined, including polyvinylidene difluoride (PVDF) in acetone (vapor pressure (VP)=30.6 kPa, boiling point (BP)=56°C) and dimethylformamide (DMF, VP=0.5 kPa, BP=152-154°C) and polyvinylpyrrolidone (PVP) in water (VP=3.2 kPa, BP=100°C), ethyl acetate (EtAc, VP=9.7 kPa, BP=77°C), and methanol (MeOH, VP=13.0 kPa, BP=65°C). The PVDF/acetone solutions produced mixtures that dried almost immediately upon exposure to air and were extremely brittle, and were thus determined to be unsuitable for our application. PVDF/DMF, PVP/water, and PVP/EtAc mixtures all produced drying times that would require each print layer to sit for over 30 min each, deemed too high. However, the methanol with a vapor pressure higher than those solvents (but lower than acetone) allowed for enough working time to load the wet pastes in a syringe for printing (1-2 min), but dried rapidly enough that solidification advanced to the point of being able to support a

next layer in DIW in under approximately 10 min.

The structures of the components of the solvent-polymer binder system used in this work are shown in Figure 2.2. PVP with molecular weight values of 10, 40, 55, and 1,300 kDa were purchased from Millipore Sigma as a solid white powder. Methanol (MeOH) was purchased from VWR. These materials were used without further purification. The molecular weight of PVP is expected to impact the binder viscosity, and thus provide a tuning parameter for the overall suspension viscosity.

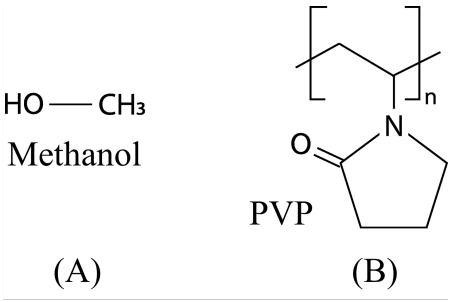

Figure 2.2: The chemical structures of the components in the solvent-polymer system, (A) methanol and (B) polyvinylpyrrolidone (PVP).

The density of PVP (1.2 g/mL) was used to calculate the mass needed to mix a 30 vol% PVP in MeOH solution for experimentation. Each solution was contained in a capped glass bottle with at minimum two layers of parafilm around the cap and bottle interface to minimize solvent evaporation. Solutions were allowed to mix overnight with the aid of stir bars at a moderate speed.

2.2.2 Photocurable System

A mixture of the monomers BisGMA and TEGDMA (structures in Figure 2.3) is a well-studied photocurable system, particularly in dental restorative applications and with inorganic fillers [70, 67, 73, 69]. Since dental composites have some similar demands as energetic materials, such as high particle content and fast curing, we selected these compounds for this study. BisGMA and TEGDMA, and the photoinitiator 1-hydroxycyclohexyl phenyl

ketone (commercially sold as Irgacure 184, compatible with acrylate and vinyl monomers [74]) were all purchased from Millipore Sigma and used without further purification.

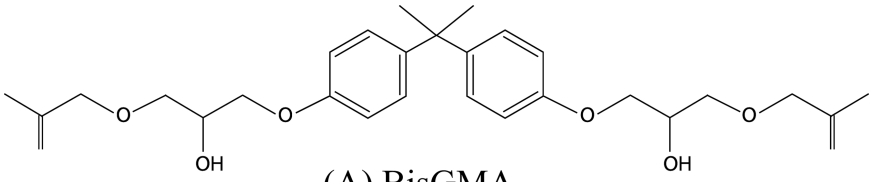

(A) BisGMA

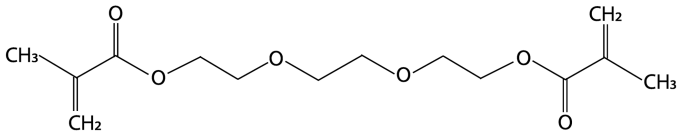

(B) TEGDMA

Figure 2.3: The chemical structures of the monomers in the photocurable system, (A) BisGMA and (B) the diluent monomer TEGDMA.

Mixtures with BisGMA and TEGDMA and other dimethacrylates or photocurable monomers are often defined using weight ratio or weight percent (wt%) [66]. The BisGMA and TEGDMA monomers were mixed in weight ratios of 1:2, 1:1, 2:1, and 4:1, with 1.0 wt% photoinitiator. These ratios were chosen to provide a range of viscosities with TEGDMA acting as a diluent for the highly viscous BisGMA. Each solution was contained in a capped glass bottle coated with Kapton tape and covered in foil to minimize premature light exposure. Solutions were allowed to mix overnight with the aid of stir bars.

2.2.3 Zero Shear Viscosity

Zero shear viscosity, represented by η_0 [Pa·s], is a rheological value commonly used to characterize the basic flow properties of polymer binders. It is formally defined as the viscosity of a fluid as the applied shear rate approaches zero and is governed by the equation [75]:

$$\eta_0 = \frac{\sigma}{\dot{\gamma}}\Big|_{\dot{\gamma}\to 0}$$

where shear stress is σ [Pa] and shear rate is $\dot{\gamma}$ [s^{-1}]. The zero shear viscosity of both polymer-solvent and photocurable binder systems were determined using a TA Instruments DHR-3 rheometer. These experiments were run using a concentric cylinder and bob geometry on all binders with the exception of the highest viscosity binders, pure BisGMA, 4:1 BisGMA:TEGDMA, and 1,300 kDa molecular weight PVP, which were all run using a 40 mm diameter upper conical plate of 2° incline geometry and a smooth bottom 40 mm diameter plate. A flow sweep procedure with the shear rate ranging from 0.002 to 100 s^{-1} was used to generate a stress-strain plot where the derivative of the stress was used to plot η_0. A minimum of 7 points in the flat linear region of the η_0 were used and averaged with error to obtain the zero shear viscosity.

2.3 Particle Selection and Characterization Methods

Particle filler materials used in these experiments were hollow glass spheres purchased from Millipore Sigma with a reported diameter range of 9-13 μm and density of 1.1 g/mL. In this thesis, the role of binder in the systems is the focus, so the specific particle shape is not explored. Because of the consistency of the spherical shape when compared to the potential irregularities among different batches of particles with grain, plate, or rod shapes, or even irregularities within single batches of material, this work uses hard spherical particles. The glass material used is relatively inexpensive and available in many sizes, and will be valuable for future work. The hardness and surface chemistry of the glass may not be an accurate representation of energetic crystals, however it is sufficient to develop a baseline understanding of highy loaded suspensions and is a cost-effective and reliable system.

2.3.1 Laser Particle Sizing

Because of its ability to accommodate particles with diameters from 0.01 up to 3,500 μm [76] (unlike dynamic light scattering which typically measures from nm up to only a few μm [77]), laser particle sizing was used to verify the size range of the particles to be used.

Typical output of these experiments include size distribution based on volume density, along with Dv(10), Dv(50), and Dv(90) values, or the volume distribution values. This means that 10% of the particles are smaller than the Dv(10), and similarly 50% and 90% for the Dv(50) and Dv(90) output values, respectively. While a single particle size average value would at least give an inclination of the general size scale, when considering the previously discussed importance of particle size distribution and packing fraction in high-solids suspensions, specific distribution information can help to shed light on trends in viscoelastic behavior.

The size range of the hollow glass microspheres was analyzed using laser scattering with a Malvern Analytical Particle Sizer 3000 for the glass spheres in water. Particle refractive index was assumed to be 1.544 and dispersant refractive index was 1.330 with particle absorption index set at 0.001. The solution was sonicated for 30 sec prior to beginning laser measurements.

2.3.2 Scanning Electron Microscopy

While laser scattering can give good quantitative size distribution data, images of particle surface and morphology can also provide valuable information about particle characteristics, including potential deformation or breakage. Samples of the glass microspheres were prepared for imaging by mounting with carbon tape onto aluminum stubs and sputter coating with a Hummer 6 gold/palladium sputter coater. Scanning electron microscopy (SEM) micrographs were captured using a Zeiss Ultra60 (Carl Zeiss NTS, LLC North America) field emission scanning electron microscope at a 3-5 kV operating voltage.

2.4 Results

2.4.1 Zero Shear Viscosity of Binder Systems

Results of the zero shear viscosity tests are provided in Tables 2.1 and 2.2. Both binder systems cover a wide range of viscosities, with PVP in methanol solutions ranging from

0.0196 to 366.6 Pa·s and the photocurable monomers ranging from 0.0072 to 637.4 Pa·s. This provides us with a broad basis over which to develop binders for DIW.

Table 2.1: Table of zero-shear viscosities for polymer-solvent binders with 30 vol% PVP of specified molecular weight in methanol.

M_w (kDa)	Viscosity (Pa·s)
10	0.0196 ± 0.0009
40	0.1082 ± 0.0035
55	0.1200 ± 0.0060
1,300	366.6 ± 24.5

Table 2.2: Table of zero shear viscosities for photocurable binders, including the pure components and specified ratios of BisGMA:TEGDMA with 1 wt% photoinitiator.

BisGMA:TEGDMA	Viscosity (Pa·s)
Pure TEGDMA	0.0072 ± 0.0008
1:2	0.0479 ± 0.0012
1:1	0.1605 ± 0.0069
2:1	0.9600 ± 0.0306
4:1	5.592 ± 0.158
Pure BisGMA	637.4 ± 16.5

The viscosity of the PVP solution increases as the molecular weight increases, as seen in Figure 2.4, with a particularly high viscosity obtained at 1,300 kDa molecular weight, which is typical for polymer solutions. For the UV curable monomer system, the viscosity increases with increasing amounts of the more viscous component, BisGMA, with an almost linear trend of log(viscosity) versus weight percent of BisGMA as seen in Figure 2.5. This is to be expected, as there is no entanglement in these monomers and the relationship between composition and viscosity will be close to a simple average of the two components.

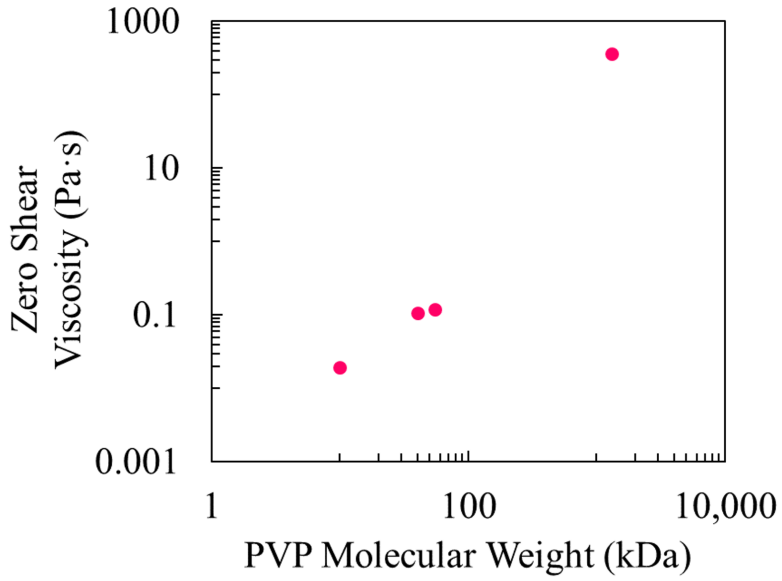

Figure 2.4: Zero shear viscosities for 30 vol% PVP in methanol polymer-solvent binders.

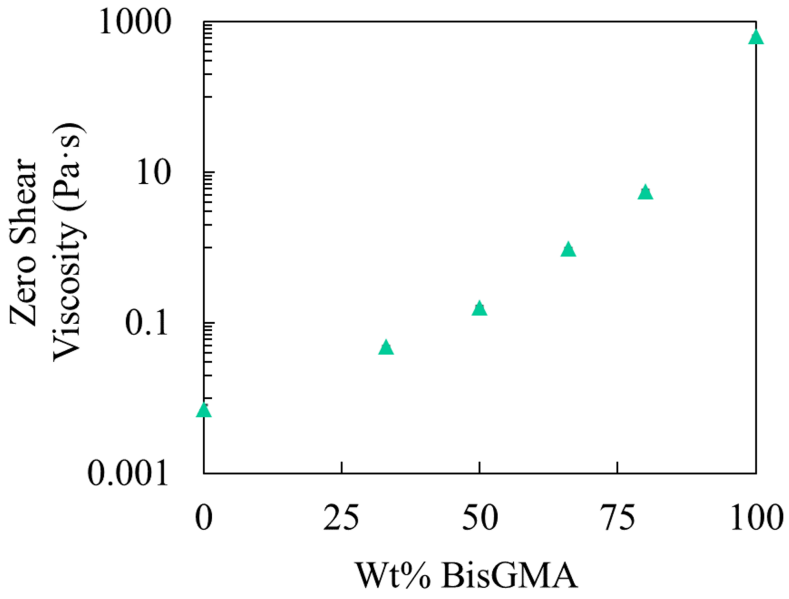

Figure 2.5: Zero shear viscosities for the BisGMA:TEGDMA photocurable binders.

2.4.2 Particle Characterization

Results from the laser diffraction particle size analysis are shown in Figure 2.6. Size distribution values from the diffraction analysis are as follows: Dv(10) = 5.35 μm, Dv(50) = 11.7 μm, and Dv(90) = 23.0 μm. The full size range covers a slightly larger range than the manufacturer's reported size range of 9-13 μm. The distribution is monomodal and polydisperse. The particle size distribution can be further visualized in the SEM micrograph of the hollow glass microspheres in Figure 2.7. Particles are spherical for the most part, with a few instances of hollow sphere breakage. SEM imaging over a much larger area (approximately 1.2 mm^2) of particulate indicated that particle breakage, while present, was similar to that seen in this image and was never greater than 3% of the particles in the image, therefore the particles are assumed to be spherical when analyzing the results.

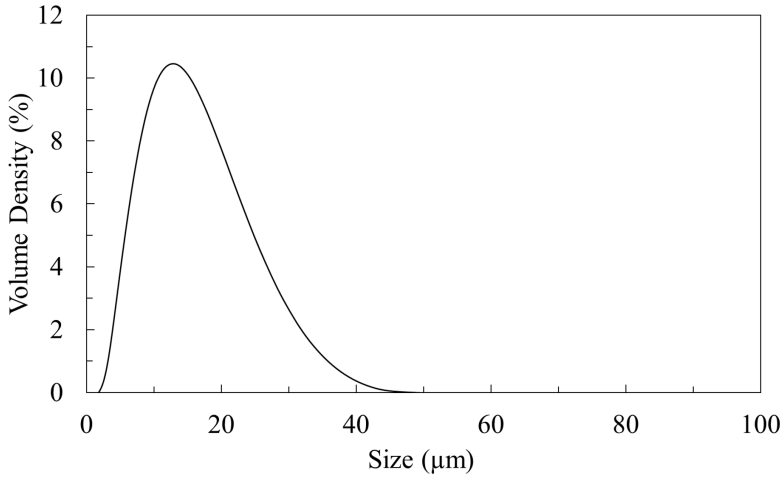

Figure 2.6: Laser diffraction measurement results showing the quantitative particle size distribution of the glass microspheres.

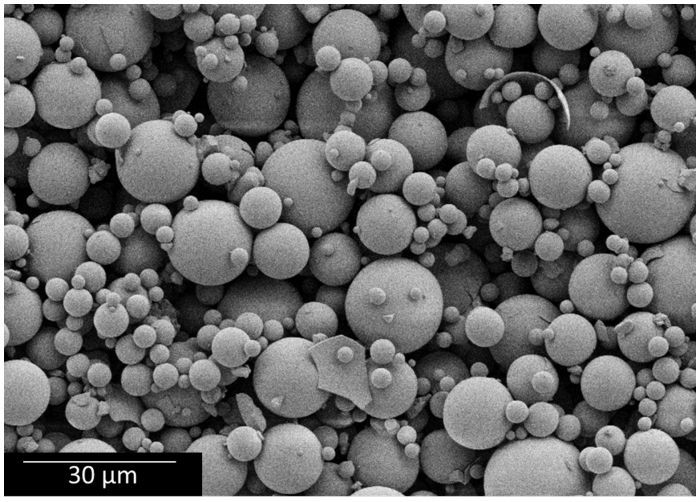

Figure 2.7: SEM micrograph of the glass microspheres qualitatively showing the size distribution.

2.4.3 Conclusions

This chapter outlined the basic considerations of solvent evaporation and photocurable binders and discussed the rationale behind the choices of PVP/methanol and BisGMA/TEGDMA systems for this work. Zero shear viscosity measurements showed that varying the molecular weight of PVP and varying the ratio of BisGMA to the diluent monomer TEGDMA were effective ways to vary the viscosities of both binder systems. Characterization of the glass microspheres via laser particle sizing showed that the distribution is monomodal and polydisperse with an experimental particle size range slightly wider than the reported 9-13 μm diameter. SEM imaging verified the assumption of spherical particles in this work.

CHAPTER 3

RHEOLOGY AND PRINTABILITY OF HIGH-SOLIDS SUSPENSIONS

3.1 Background

The viscosity of suspensions that are used as DIW inks prior to their solidification is directly related to their printability. Understanding the viscoelastic properties of inks allows for additional tailoring of the printing process to achieve uniform, high quality prints able to flow well through the print nozzle but still maintain their shape after extrusion. As discussed in section 1.1.1, the highly viscous nature of high-solids suspensions can make working with these materials a challenge, both for mixing and for measuring viscoelastic flow properties, leading to complex experimental set-up and data interpretation. Rheological instrumentation itself can interfere with accurate measurement of the inherent suspension properties. This chapter focuses on the development and implementation of mixing processes and rheological characterization of our high-solids suspensions and uses those methods to examine the tie between suspension viscosity and printing, specifically flow consistency and line prints.

3.2 Methods

3.2.1 Mixing

Traditional nutating and shaker mixers are tabletop instruments that employ rocking/rotating and shaking motions, respectively, to promote mixing of solutions in individual vessels secured to their surfaces. However, these techniques proved too gentle to incorporate the high amounts of particles into the relatively high viscosity binders necessary for these experiments. It was also determined that Resonant Acoustic Mixing (RAM), despite its use of high resonant frequencies in combination with rapid uniaxial motion to impart much

more powerful mixing energy than a nutator or shaker, was also unable to fully mix the highly loaded suspensions. This was evidenced both by visually noting that the dye added to the mixture was not fully incorporated and by observing inconsistent material output from the syringes during printing (via preliminary flow tests, a procedure discussed later in this chapter). The FlackTek Dual Asymmetric Centrifuge (DAC), however, led to more consistent dye incorporation and extrusion through the printer nozzle.

The FlackTek DAC is a bladeless mixing technology that houses samples in individual, capped mixing vessels and generates high mixing power through both centrifugal and axial rotating motions [78]. When using this technology for mixtures with high solid content, these rotations also generate high amounts of interparticle contact that promotes suspension mixing. The inexpensive and disposable sample vessels eliminate the need to clean blades that are typically found in Brabender-type machinery. The key advantage of this feature is that, despite best practices with cleaning of the reusable steel blades and containment units, buildup of energetic residue in cracks or crevices can pose a major hazard. The bladeless technology along with the high speed centrifugal motion has the added benefit of minimizing air pockets and voids during the mixing process [78], which also is beneficial for energetic applications, as a major goal in AMEMs is to eliminate voids that can cause hot spot formation.

However, though the interparticle contact during rotations promotes mixing, this friction can also cause rapid temperature increases. Therefore, special precautions should be taken when using this high speed mixing technology for energetic constituents due to heat generation. Additionally, solvent-based high-solids suspensions may be more sensitive to the heat that is formed during mixing than the photocurable binders due to increased vapor pressure at higher temperatures, which leads to increased solvent evaporation and a change in the formulation composition. Thus, for the polymer-solvent system, proper containment methods were taken into consideration to account for any potential solvent loss.

All suspensions in this work were mixed in either 150 mL polypropylene (PP) cups or 20 mL glass vials in a FlackTek DAC 400.2 VAC - LR Programmable SpeedMixer for 3 min total at two speeds, first 30 s at 1000 rpm followed by 150 s at 1500 rpm. The short low speed mixing step was designed to wet the particles and incorporate them into the binder, and the subsequent higher speed step was designed to fully complete the mixing process and maximize the homogeneity of the final suspension. All solvent-based systems were sealed with at least two layers of parafilm to minimize the loss of solvent, and all photocurable systems were covered either with aluminum foil or Kapton tape (or both) to minimize premature curing from light exposure.

3.2.2 Rheology

Rheology is valuable for exploring the viscoelastic properties of non-Newtonian polymeric materials. Besides being able to extract viscosity data (as demonstrated in section 2.4.1), other important parameters in rheological analysis are the storage and loss moduli (G' and G", respectively), collectively referred to as the complex modulus. G' is a measurement of the elastic response of a material, i.e. the stiffness (or solid-like behavior), while G" is a measurement of the viscous response, i.e. the liquid-like behavior. When G'>G", the material is considered a viscoelastic solid, but when the opposite is true (G'<G"), the material is said to be a viscoelastic liquid [25]. The use of these properties to characterize high-solids suspensions are discussed in further detail later in this section.

One of the most widely used types of rheological testing is oscillatory, which places the sample of interest between two parallel plates and oscillates the top one back and forth to impose a sinusoidal stress-strain response in the material. Development of a good rheological test regimen involves selection of proper rheometer geometries (i.e. selecting a sample holder that appropriately accommodates the sample type), understanding the limits of the linear viscoelastic regime (LVR), and determining the time stability (i.e. understanding whether or not the material sample changes over time despite constant test conditions).

These considerations are discussed in this section along with the development of the rheology test procedures used in this work.

Geometry Selection for High-Solids Suspensions

When working with high-solids suspensions, selection of the rheometer geometry (i.e. the sample holder) is especially important because of the challenging nature of working with these materials. Wall slip is the phenomenon of forming a low-viscosity layer in a sample near the rheometer plates during testing of particle suspensions, and the low viscosity layer formed near the plate surfaces is often referred to as the apparent slip layer [21, 79, 80]. Potential wall slip due to high volumes of large particles can be targeted by using parallel plates with a crosshatched (rather than smooth) surface to prevent an apparent slip layer from causing measurement error.

When working with the suspensions, it was found that the 40 mm smooth parallel plates, shown in Figure 3.1A, when loaded with the highly viscous samples used in this work, not only did not provide adequate resistance to wall slip (tested by tracking the movement of marks on the plates and sample), but were also very difficult to bring to the proper 1 mm loading gap. Not only did this impart forces nearing instrument axial force limits, but even with a gap override, the recorded torque values during oscillatory testing also approached instrument limits, likely due to such a high geometry surface area. Thus, plates of a smaller 20 mm diameter, shown in Figure 3.1B, were acquired to make it easier to reach the loading gap and to reduce axial force and torque values. These plates additionally had crosshatched surfaces to prevent formation of a binder-only layer and thus minimizing wall slip.

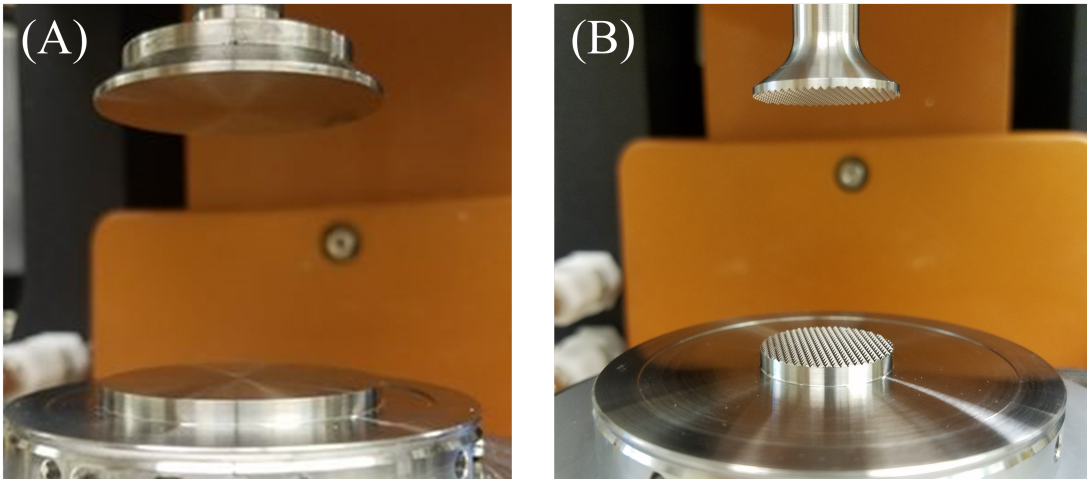

Figure 3.1: Photographs of (A) the 40 mm smooth parallel rheometer plates and (B) the 20 mm crosshatched rheometer plates, both at the loading gap prior to sample loading.

Linear Viscoelastic Regime

The LVR refers to the conditions under which a viscoelastic material maintains linear properties despite changing stresses and strains imposed on it. In other words, the storage and loss moduli (G' and G", respectively) are independent of any change in the oscillatory movement (the back and forth shearing motion of the top plate) [25]. It is important to determine the limits of the LVR so that further tests are run under conditions where the internal structure of the material is maintained. Additionally, for our application, the LVR tends to be very small for high-solids suspensions, so the upper and lower limits of each new formulation must be tested individually.

One way to determine a workable strain range within the LVR is to do a basic strain amplitude sweep and plot G' as a function of strain, as illustrated in Figure 3.2. The LVR is then defined to be the horizontal linear region of the plot, as labeled in the figure. Oscillatory tests should be run only using strain values that fall within that determined range to ensure that the properties are independent of the changing stresses and strains [25]. The LVR for materials at the lower and upper bounds of the volume percentages used

in these experiments were determined using the TA Instruments DHR-3 rheometer with 20 mm crosshatched parallel plates and a basic strain sweep at 1 Hz from 0.001 % to 1.0 % strain.

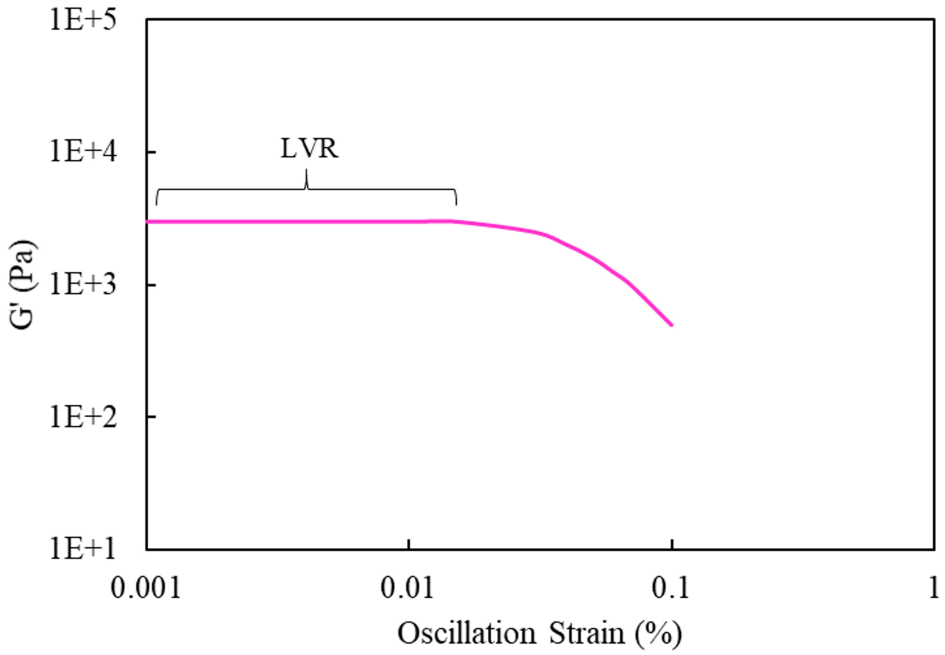

Figure 3.2: Illustration of using a strain sweep to determine the linear viscoelastic region of a viscoelastic fluid or suspension.

Material Stability Over Time

Particularly when working with the solvent system, understanding the stability of the material under rheological shear over time is valuable in making sure measurements are capturing actual material behavior and not just the solvent evaporation process. Time stability of the high-solids suspensions were obtained through a time sweep at 0.01% strain and 1 Hz frequency.

Oscillation Frequency Test Procedure

Oscillation frequency tests use the previously described sinusoidal strain variation to measure the stress response in the material as function of the angular frequency while oscillating to a constant strain value. Oscillation frequency tests in these experiments were used to gather complex viscosity, storage modulus (G'), and loss modulus (G") of each formulation using the TA Instruments DHR-3 with 20 mm crosshatched parallel plates. In all cases the initial loading gap was set to 1 mm and the solvent trap was in place, with axial force adjustment at 0.05 N compression. Oscillation frequency tests were run at 0.01% strain and 0.1 to 100 rad/s angular frequency range at ambient temperature on all slurries to characterize the viscoelastic behavior.

3.2.3 Flow Tests

To understand printer flow properties of each suspension type, a simple test was developed that measures the suspension flow over set time intervals throughout the printing process, with the aim to allow for comparison between different systems and formulations. Flow tests were performed using a Hyrel Hydra 640 3D printer and SDSXT-30 printer head (which uses a stepping motor with a gear reduction system) with 30 cc plastic syringes equipped with 14G Nordson SmoothFlow Tapered luer nozzles. Prior to the first run, the syringe was primed for 0.53 seconds, and the mass extruded in a 42 second time window was measured. This time corresponds to one line of the printing line tests which will be discussed in a later section. The extrudate was collected in weigh boats and massed immediately. Multiple 42 second runs were performed for each formulation, corresponding to the lines in the line tests. The change in the mass extruded in 42 seconds from the start to end of the experiment was measured. The GCode for this test can be found in Appendix A.1.

3.2.4 Line Tests

To further analyze the variation of suspension flow from the printer nozzle under constant motor/extrusion rate, single layer line tests were used to measure the width of the deposited material. This line test (developed and implemented by Andrew Boddorff) was performed on suspensions composed of 61.4 vol% glass microspheres in the 55 kDa and 1,300 kDa PVP binders and the 2:1 BisGMA:TEGDMA binder (65.7 wt% and 60.6 wt%, respectively for PVP and BisGMA:TEGDMA suspensions). Using the same Hyrel Hydra printer setup from the flow tests, we deposit a snaking single layer line pattern (Figure 3.3A) onto a transparent plastic sheet and quantify the line width via post-print image analysis. Before the start of each print, the extruder performs a short prime action to begin the material extrusion. The printer head then moves at a speed of 5 mm/s for a length of 200 mm, extruding material at a motor rate 30 pulses/μL with a layer height of 1 mm. At the end of the first line, the printer head moves perpendicularly for 10 mm then prints the same 200 mm line parallel to the initial print. This repeats until all lines are deposited and the whole print is done without interruption. Upon finishing the print, the head is moved off to the side and an unprime action is performed to stop the extrusion of material. For the UV binder system, the lines are then cured with a 365 nm UV light pen that retraces the printing path from a short distance. To measure the line width, images are taken of each line in 10 mm segments. The resultant images are then color thresholded with ImageJ to segment the image. Approximately every 400 μm, the pixels across the line are counted as shown by yellow lines in Figure 3.3B. A calibration slide is used for each set of images to convert the pixels to microns. The GCode for the line tests can be found in Appendix A.2.

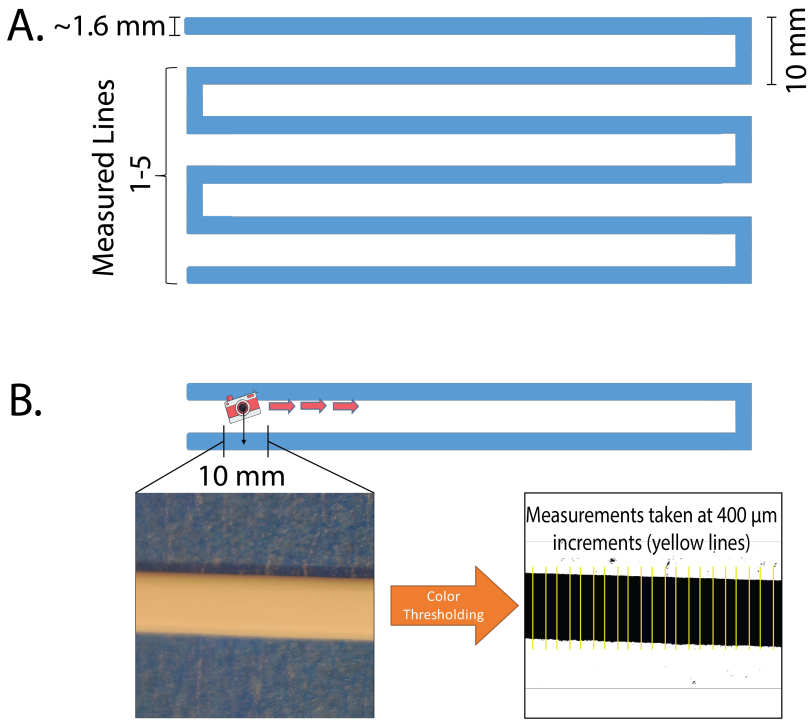

Figure 3.3: Line test method showing (A) the snaking pattern of the deposited lines used to measure the consistency of the line width and (B) a depiction of the imaging process showing an example of a raw (left) and thresholded image (right) used for pixel counting. Image courtesy of Andrew Boddorff.

3.3 Results

3.3.1 Effect of Particle Loading on Rheology of Suspensions

To study the effect of particle loading on the suspension rheology, we examined high-solids suspensions containing 61-69 vol% glass microspheres in two moderate viscosity binders: 1) 30 vol% 55 kDa PVP in methanol, and 2) 2:1 BisGMA:TEGDMA. This range of particle loadings was selected because it is most relevant for our application.

Linear Viscoelastic Regime

Strain sweeps showing the storage modulus G' as a function of oscillation strain for the 61.0 and 69.0 vol% microspheres in the solvent and photocurable binders are shown in Figures 3.4 and 3.5, respectively. The 61.0 and 69.0 vol% samples were analyzed to determine the LVR for the highest and lowest particle content and bracket our range.

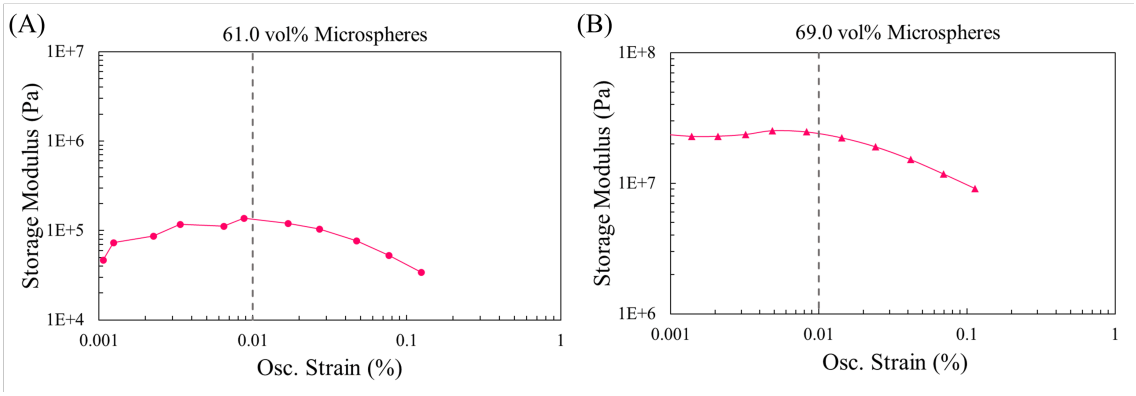

Figure 3.4: Storage modulus as a function of oscillation strain (to determine the LVR) in the 55 kDa PVP in methanol polymer-solvent binder for (A) 61.0 vol% microspheres and (B) 69.0 vol% microspheres.

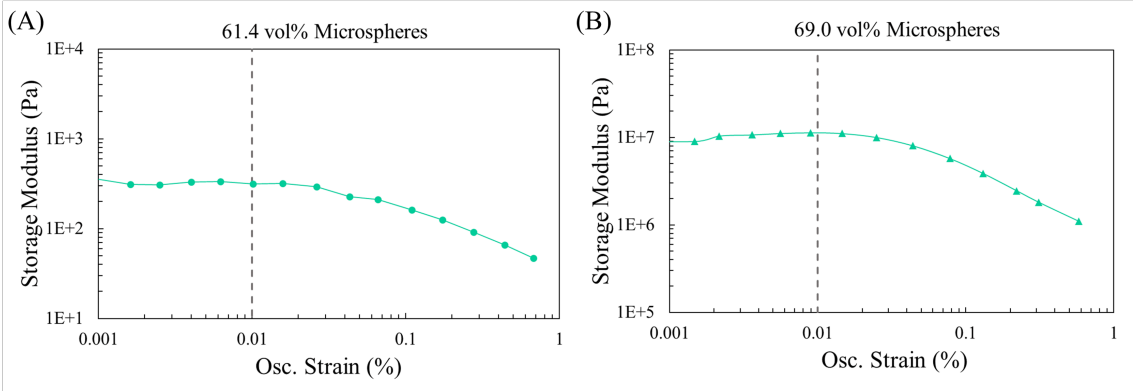

Figure 3.5: Storage modulus as a function of oscillation strain (to determine the LVR) in 55 kDa PVP in the 2:1 BisGMA:TEGDMA photocurable binder for (A) 61.4 vol% microspheres and (B) 69.0 vol% microspheres.

While the decrease in G' at high strain values clearly indicates the end of the LVR, it is also noteworthy that for the less stiff suspensions, strains at the lower extreme do not always produce a linear regime. This is particularly visible for the 61.0 vol% solvent system in Figure 3.4, where the initial strain region of 0.001 to 0.003 % lacks stability. It was determined that 0.01 % strain, represented by the dashed vertical line in each figure, lies reasonably within the LVR for each suspension and was therefore used for subsequent time sweeps and oscillation frequency testing.

Time Sweep Rheology

Figure 3.6 shows the results from the time sweep of the 61.0 vol% microspheres in the 55 kDa PVP in methanol binder. Despite the use of the solvent trap, the methanol still is exposed to the air in the trap, and the initial rise in viscosity is attributed to solvent evaporation, additionally evidenced by the dryness of the suspension upon removal from the rheometer after the test. The rapid initial evaporation rate seen in this time test is beneficial for the DIW process, but to account for it in rheological studies, subsequent testing was designed to last as short a time interval as reasonably possible, and all tests were run under the same conditions to make data comparable.

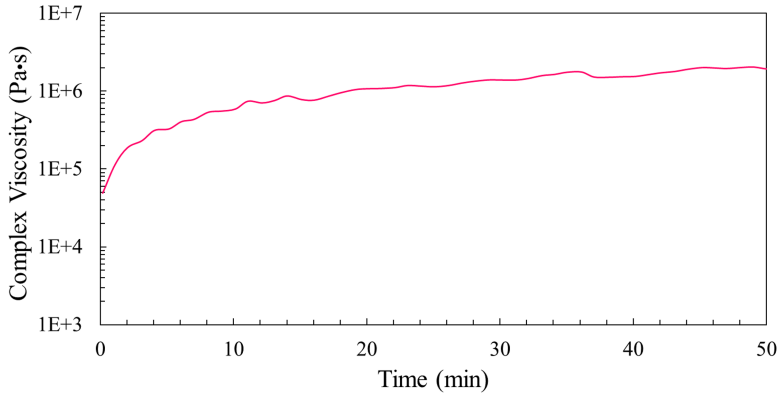

Figure 3.6: Complex viscosity as a function of time for 61.0 vol% microspheres in the 55 kDa PVP in methanol binder.

Oscillation Frequency Rheology

Figure 3.7 shows the viscosity measured at 1 rad/s as a function of vol% particles for suspensions with the 30 vol% 55 kDa PVP in methanol binder. The jamming transition is visible, as seen by the increase in viscosity at approximately 67.0 vol% particles. This corresponds well to the theoretical jamming transition at 0.64 volume fraction for random close-packed spheres [30], and likely differs due to our particle size distribution not being uniformly monomodal [33]. Above the jamming transition, the particle suspensions were not easily printable with our printer set-up and motor. This indicates that a formulation should be selected with a volume fraction below approximately 66.0% for monomodal 10 μm spheres when using the PVP/methanol 55 kDa 30 vol% binder suspension. For further studies, 61.4 vol% particles were used, which are well within the lower viscosity range.

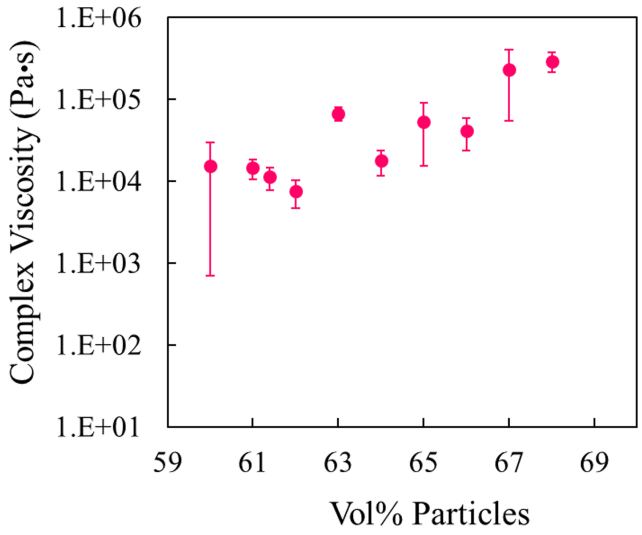

Figure 3.7: Complex viscosity at 1 rad/s angular frequency as a function of volume percent particles for microspheres in the polymer-solvent 30 vol% 55 kDa PVP in methanol binder.

A similar study was performed with the 2:1 BisGMA:TEGDMA photocurable monomers, and these results are shown in Figure 3.8. The viscosity plateaus at the higher volume per-

cent particles beyond about 67 vol% particle loading. Similar to the solvent system, this likely corresponds to the jamming transition for the glass microspheres. What is notable with the UV-curable monomers in contrast to the PVP solvent system is the clear trend of increasing viscosity starting at lower (61-66) volume percentages with less scatter in the results. This may be due to evaporation occurring in the solvent samples that is hard to control. With so little solvent in these suspensions, even a small amount of evaporation can lead to strong increases in the viscosity and lead to the scatter seen in the PVP binder samples. Careful design of the mixing process minimizes solvent evaporation to maintain controllable rheology for printing, but future work with this system could aim to further optimize solvent control via novel syringe loading techniques.

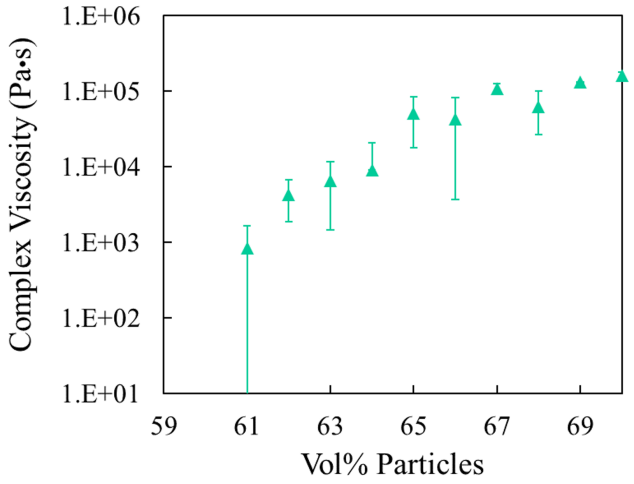

Figure 3.8: Complex viscosity at 1 rad/s angular frequency as a function of volume percent particles for microspheres in the photocurable 2:1 BisGMA:TEGDMA binder.

3.3.2 Effect of Binder Choice on Rheology and Flow of Suspensions

Effect of Molecular Weight on Rheology of Solvent Binders

As the molecular weight of a polymer increases, the greater the increase in viscosity from a given concentration of the polymer and past a sufficiently high viscosity, entanglements between polymer chains serve to increase the viscosity even more sharply with concentra-

tion. In the presence of high particle loadings, the increase in viscosity due to the increase in the polymer molecular weight is still present, as can be seen in Figure 3.9, which shows the complex viscosity of 61.4 vol% hollow glass spheres in a 30 vol% PVP in methanol binder. For the 10 kDa PVP molecular weight, the viscosity displays a value of 563 Pa·s at 1 rad/s, while viscosity at 1 rad/s increases to 4.3 x 10^5 Pa·s for 1,300 kDa PVP, three orders of magnitude higher.

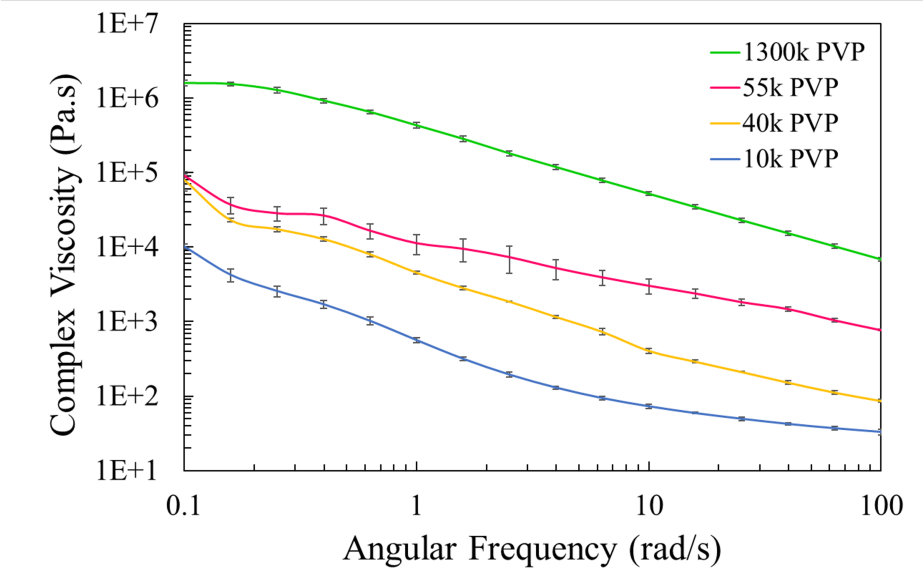

Figure 3.9: Complex viscosity as a function of angular frequency for the 61.4 vol% hollow microspheres data in each of the 30 vol% PVP in methanol binders, 10 kDa PVP (blue), 40 kDa PVP (yellow), 55 kDa PVP (pink), and 1,300 kDa PVP (green).

Effect of BisGMA:TEGDMA Ratio on Rheology of Photocurable Binders

Since the BisGMA has a viscosity that is two orders of magnitude higher than the TEGDMA, a significant increase in the viscosity of the binders was observed when the amount of BisGMA was increased (Figure 2.5). To determine the effect of this increase on the suspension rheology, we examined the four different ratios, 1:2, 1:1, 2:1 and 4:1 BisGMA:TEGDMA with 61.4 vol% particles. As can be seen in Figure 3.10, there is a slight increase in the viscosity as the amount of BisGMA in the mixture increases, but it is barely significant

given the size of the error bars. Specifically, the 4:1 Bis-GMA:TEGDMA is significantly different than the 1:1 and 1:2, but it is within error of the 2:1 BisGMA:TEGDMA. This indicates that, for these mixtures of monomers with particles, the particle content is the primary driver for how the suspension flows, in contrast to the behavior seen with the high molecular weight polymers in solvents.

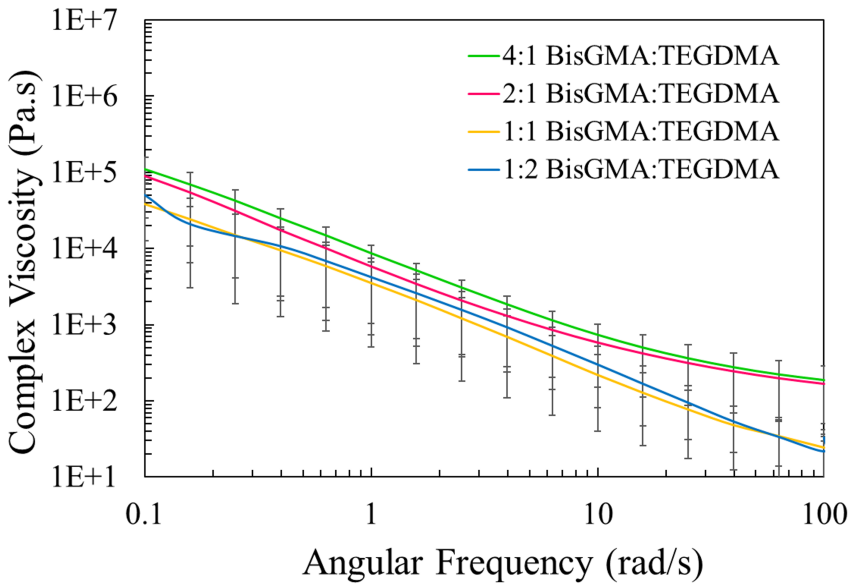

Figure 3.10: Complex viscosity as a function of angular frequency for the 61.4 vol% hollow microspheres data in each of the the photocurable binders, 1:2 BisGMA:TEGDMA (blue), 1:1 BisGMA:TEGDMA (yellow), 2:1 BisGMA:TEGDMA (pink), and 4:1 Bis-GMA:TEGDMA (green).

Effect of Molecular Weight on Flow of Solvent Binders

Flow tests of these different solutions help to better understand the effect of the molecular weight on the flow of these suspensions through the syringe and nozzle during printing. Figure 3.11 shows the extrusion rate plotted against the line number (corresponding to the line tests) for the 10 kDa, 55 kDa and 1,300 kDa PVP. It is clear from these results that the 1300 kDa PVP is not printable. The extrusion rate increases over the first 4 lines, but

then decays off as the print continues, always staying below about 0.05 g/min. The 10 kDa and 55 kDa PVP reach the steady state extrusion rate of 0.2 g/min by the second line and maintain that flow rate up to 23 lines, indicating that they are good candidates for printing with respect to flow rate consistency.

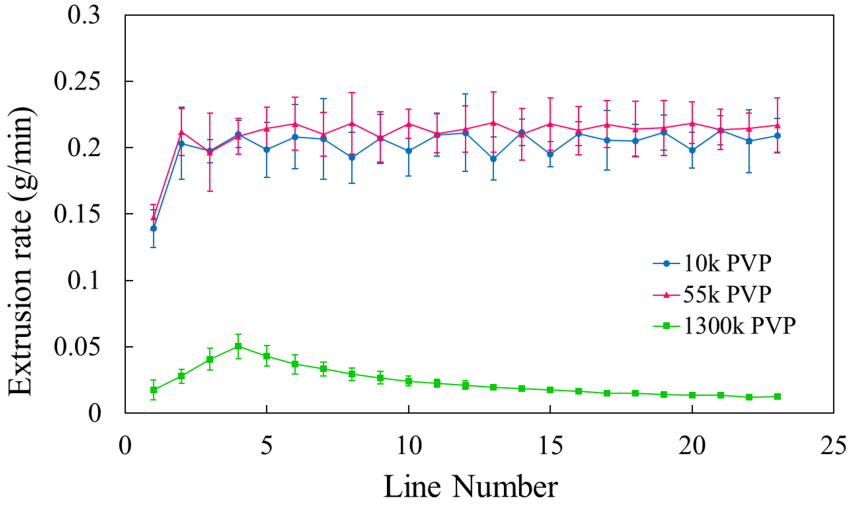

Figure 3.11: Extrusion rate as a function of line number for the 61.4 vol% hollow glass microspheres in each of the 30 vol% PVP in methanol binders, 10 kDa PVP (blue), 55 kDa PVP (pink), and 1,300 kDa PVP (green).

Effect of BisGMA:TEGDMA Ratio on Flow of Photocurable Binders

Flow tests were also performed on the four different ratios of BisGMA:TEGDMA and these are plotted in Figure 3.12. For the three ratios with the lowest amount of BisGMA, steady state was reached relatively quickly, by about lines 3-5, while for the highest ratio of Bis-GMA:TEGDMA, steady state was not reached until line 17. The cause of the different behavior for the 4:1 sample is unknown, though it is not caused by aging of the sample as all 3 repeats, which were done consecutively with the same syringe, showed similar behavior. As the 2:1 BisGMA:TEGDMA showed acceptable start-up behavior and consistent flow and it is known from the literature to be a good ratio for curing[24,25,30], this mixture was used for further testing.

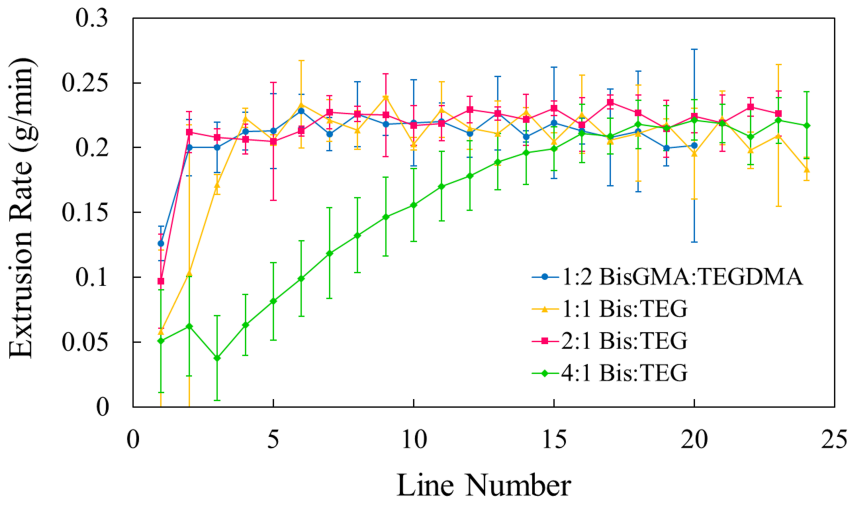

Figure 3.12: Extrusion rate as a function of line number for the 61.4 vol% hollow glass microspheres in each of the photocurable binders, 1:2 BisGMA:TEGDMA (blue), 1:1 Bis-GMA:TEGDMA (yellow), 2:1 BisGMA:TEGDMA (pink), and 4:1 BisGMA:TEGDMA (green).

3.3.3 Effect of Binder System Type on Rheology and Printability of Suspensions

A major objective of this work is to understand the difference in the rheology and flow of the selected solvent evaporation and polymerization binders (PVP in methanol versus Bis-GMA:TEGDMA). To do this, we took a closer look at the rheology and print consistency to compare the two systems, particularly focusing on the 61.4 vol% particle cases. This section focuses on comparing the two binder system types: solvent-based vs. photocurable binders.

Rheology to Compare Solvent and Photocurable Binder Systems

The viscosities of the two types of systems are compared in Figure 3.13. Interestingly, the two formulations show similar viscosities, despite being selected for properties other than viscosity. They diverge at higher angular frequencies, with the BisGMA:TEGDMA mixture showing a lower viscosity. This could be explained by the difference in molecular

structure of these systems, the small molecules in the BisGMA:TEGDMA system may be more mobile at higher frequencies than the long polymer chains of the 55 kDa PVP, which are likely held together by entanglements, that may still disentangle with the imposed higher shears, but are unable to move to the extent that the photocurable monomers are able.

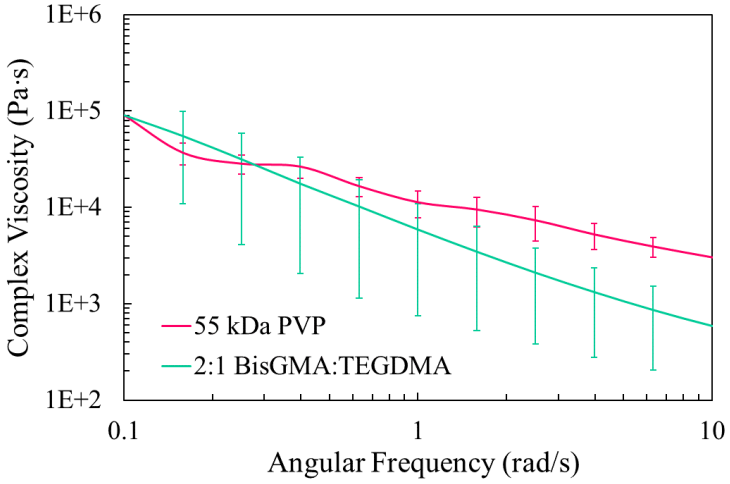

Figure 3.13: The viscosity as a function of angular frequency for 61.4 vol% particles in 30 vol% 55 kDa PVP in methanol binder (pink) and 2:1 BisGMA:TEGDMA (teal).

Line Tests to Compare Solvent and Photocurable Binder Systems

To examine their printability, line tests were performed for these two formulations. The average line width over lines 2-7 (line 1 was removed to focus on the steady state regime) was 0.79 $\pm$ 0.08 mm for 55 kDa PVP (30 vol% in methanol) and 0.99 $\pm$ 0.14 mm for 2:1 BisGMA:TEGDMA when printed with the 14G nozzle. This shows that the printing is relatively consistent from one line to another (only varying by 10% and 14% for PVP and BisGMA/TEGDMA, respectively) throughout the print. However, the line width measurements ignore areas of significant defects and only take into account the smooth printing areas. In the case of the two binders tested here, the visual quality of the prints were significantly different. As shown in Figure 3.14 A and B, the first 2-3 lines of the BisGMA:TEGDMA sample have significantly more defects. The preliminary hypothesis

is that there is less cohesion in the jet due to a lack of entanglements, leading to easier breakage for the BisGMA:TEGDMA. For comparison, Figure 3.14C shows the print for the very high molecular weight PVP (1,300 kDa). It is clear that the print quality was poor and less than half of the printing was successful. This corresponds with flow test data that show a low extrusion rate for the 1,300 kDa PVP formulation, limiting the amount of material coming out of the syringe.

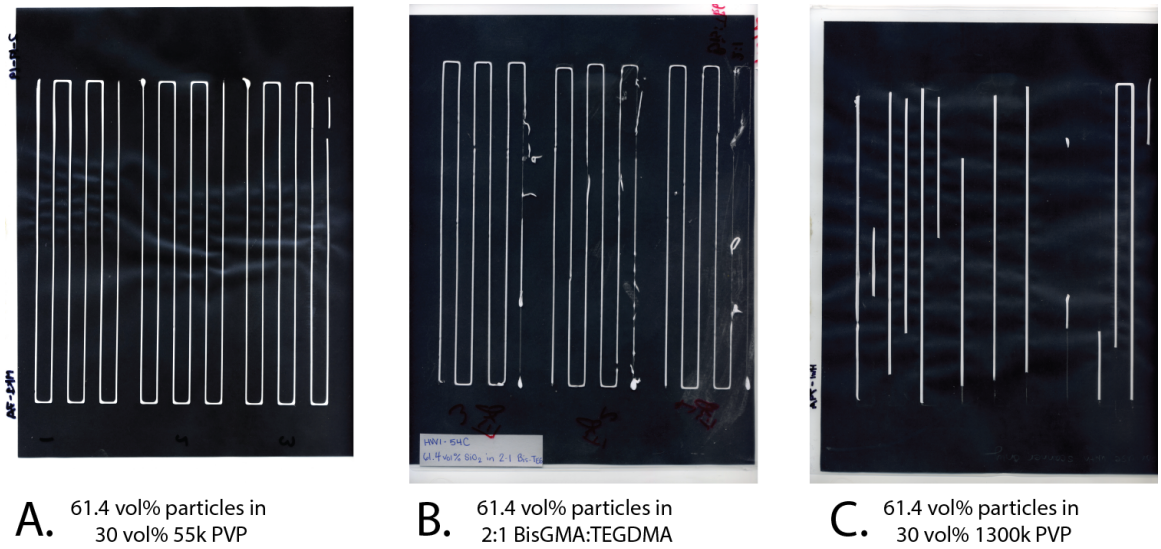

Figure 3.14: Scanned images of line tests, (A) 61.4 vol% particles in 30 vol% 55 kDa PVP, (B) 61.4 vol% particles in 2:1 BisGMA:TEGDMA, and (C) 61.4 vol% particles in 30 vol% 1,300 kDa PVP.

CHAPTER 4
PRINT QUALITY ANALYSIS

To evaluate the overall print quality and potential for continuation of studies for the two types of binder systems, surface SEMs and macroscopic cylinder prints were examined and are discussed in this chapter.

4.1 Printing Methods

All prints were done using the previously introduced Hyrel Hydra 640 3D printer and SDSXT-30 printer head (which uses a stepping motor with a gear reduction system) with 30 cc plastic syringes equipped with 14G Nordson SmoothFlow Tapered luer nozzles.

Single Layer Surface Analysis

The top surface of the cured single layer line prints (for which flow properties were discussed in chapter 3) were examined at the microscale using SEM. Images of the surface of were analyzed using ImageJ software and converted to binary images using the Threshold function. The color threshold was set so that the particles were shown as black and the binder shown as white. This was repeated for the 61.4 vol% glass microspheres in both the 55 kDa PVP system and the 2:1 BisGMA:TEGDMA system. The percentage of black area compared to white area in the image was calculated to determine the percentage area of particles.

3D Printed Cylinders

DIW was also used to print 3D objects in the form of disks using 61.4 vol% particle suspensions for the 55 kDa PVP (30 vol% in methanol) and 2:1 Bis-GMA:TEGDMA with the layer height set to 0.5 mm, extrusion rate to 45 pulses/μL, and head speed to 5 mm/s. These

parameters were optimized by trial and error to the point of achieving a self-supporting solid structure, but were not extensively studied in comparison to other print parameters.

4.2 Results

4.2.1 Single Layer Surface Analysis

The SEM micrographs of the top of the printed surfaces and their thresholded counterparts are shown in Figure 4.1. It was found that the total area of particle contents were similar between the two systems, 89.6% for 2:1 BisGMA:TEGDMA and 91.0% for 55 kDa PVP.

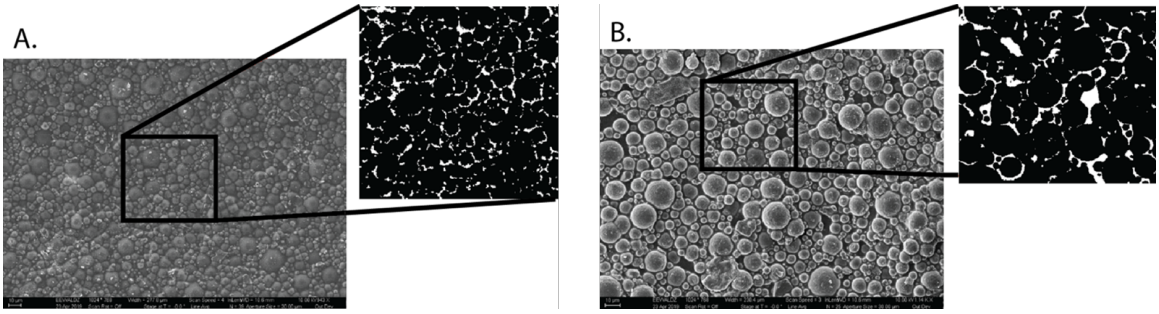

Figure 4.1: SEM micrographs of the surfaces of a prints from 61.4 vol% particles in (A) 55k PVP binder 30 vol% in methanol) and (B) 2:1 Bis-GMA:TEGDMA binder.

The main differences seen are the spacing between particles, with 55 kDa PVP system having less space between particles, but appearing to have more small particles on the surface. In the 2:1 BisGMA:TEGDMA system, larger particles along with larger spacing between particles were observed on the surface. This difference in spacing and particle distribution is possibly due to a difference in curing mechanisms/time scales. With solvent evaporation, the system solidifies quickly so the polymer and particles get locked into place immediately after printing. Whereas with a UV curing system, the sample is left uncured for a certain amount of time before being treated with UV light. This allows time for relaxation of the system and movement of particles, with smaller particles being more mobile in the matrix and settling to the surface.

4.2.2 3D Printed Cylinders

Printed disks, shown in Figure 4.2, were approximately 30 mm in diameter and 4-6 mm thick. Both disks are similar with no obvious voids, but surface heterogeneities from the printing path are visible on the sides and tops of each. Further optimization of these printing parameters could yield more uniform results, but these preliminary prints demonstrate the promise of these materials for additive manufacturing of 3D objects with solid infill.

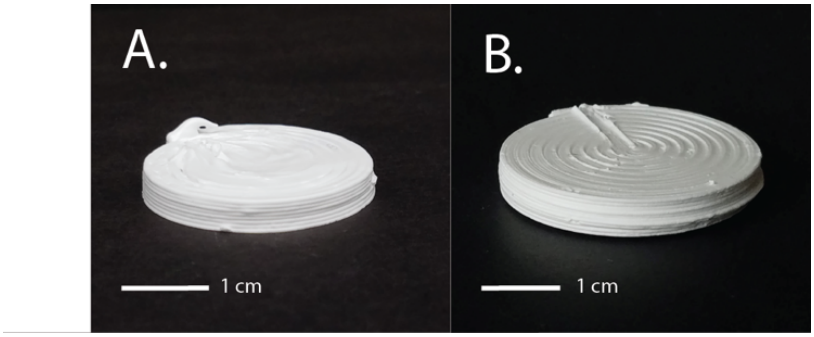

Figure 4.2: 3D printed disks of 61.4 vol% hollow glass microspheres in (A) 55k PVP binder and (B) the 2:1 BisGMA:TEGDMA binder after solidification.

CHAPTER 5
CONCLUSIONS AND FUTURE WORK

5.1 Conclusions

This work examined the rheology and printability of highly loaded silica particle suspensions in two different types of polymer binders: a high molecular weight polymer in a solvent and polymerizable monomers that were cured via UV light. The implications of individual suspension components on suspension rheology, in particular the binder component, were characterized and understood through rheological measurements and particle characterization (Objective 1). For the high molecular weight polymer binder, 30 vol% PVP in methanol, the molecular weight had a strong effect on both binder viscosity and suspension viscosity. This is contrary to the UV curable binder system, BisGMA/TEGDMA, where the ratio of the monomers only affected the binder viscosity and the particle loading primarily set the suspension viscosity.

Viscoelastic properties of particle-binder suspensions for varied particle content of glass microspheres in polymer-solvent and photocurable binder systems were measured with oscillatory rheology to show that suspension viscosity is primarily controlled by the particle volume fraction for the photocurable binder, while both the particle volume fraction and polymer molecular weight influence the viscosity in the case of the polymer-solvent binder (Objective 2). In both cases, the viscosity increased with volume fraction of particles up to approximately 67 vol%, where the jamming transition occurs and the viscosity plateaus at a high value.

Printability of both the polymer-solvent and photocurable systems was demonstrated through flow tests, line tests, and 3D printing. In both cases, the suspensions could be tuned to a printable viscosity, in the range of 1 x 10^4-1 x 10^5 Pa.s at 1 rad/s angular frequency and

printed as lines of consistent width, as well as 3D objects in the form of discs (Objective 3). These results show a flexible formulation system for preparing highly loaded suspensions of energetic particles, creating a path to the design of new high performance energetic materials, including polymer bonded explosives.

5.2 Future Work

This work lays the foundation for further work on additive manufacturing of high-solids suspensions and energetic materials. Future work may include further optimization of the printed disks with the two primary types of binders discussed here. Work may also go on to include studies of the effect of glass microsphere size and modality on suspension rheology in the different binders systems and their subsequent printability. It would also be valuable to understand the implications of changing particle type (and properties such as surface chemistry and shape) in each system. The correlation of the simulant high-solids suspensions in this work to live AMEMs should be analyzed so that the impact of this work with respect to the energetic community can be fully assessed. Finally, other potential applications that may use DIW of similar high-solids suspensions include pharmaceuticals, fuel cells, and batteries.

Appendices

APPENDIX A

GCODES

A.1 Flow Test GCode

Flow Test GCode with comments (semi-colon indicates sections commented out)

```
;***PRIME***
    M722 S10000 E5000 P1000 T11 I1 ; prime 5000 steps
    G4 S.5 ; pause to execute prime for S amount of seconds
    M722 S10000 E300 P100 T11 I1 ; reset prime so doesn't double
    G4 S.03 ; pause to execute prime reset
    ;***MATCH FLOW OF LINE***
    M723 S240 E60000 T10
    ; S is pulses per second
    ; E is number of pulses
    G4 S250 ; pause to execute flow for S amount of seconds
    ; S needs to match total time (E from M723 divided by S from M723)
    ;(repeat flow of line section as needed to provide desired duration of test)
    ;***UNPRIME***
    M721 S10000 E5000 P500 T11 I1 ; unprime 10000 steps
    G4 S.5 ; pause to execute unprime for S amount of seconds
```

Minimalist Flow Test GCode (No Commented Code)

```
M722 S10000 E5000 P1000 T11 I1
    G4 S.5
    M722 S10000 E300 P100 T11 I1
```

G4 S.03

M723 S240 E60000 T10

G4 S250

M721 S10000 E5000 P500 T11 I1

G4 S.5

NOTE: This code is compatible with the Repetrel software as of April 2019. Due to frequent software updates and new versions, alterations may need to be made to accommodate printers at other institutions.

A.2 Line Test GCode

Line Test GCode (semi-colon indicates sections commented out)

;***Select Printer Settings***

M203 X8000 Y8000 Z1000 ;set the G0 speeds to slow

G21 ; set units to millimeters

G90 ; absolute coordinates

;G0 Z30 ; drop bed to avoid collisions

G53; Turn offets off before homing.

G28 X0 Y0 ; home X and Y

M221 T11 S1 P30 W1.6 Z1; set flow conditions

; T indicates the printer head to be used

; S is the flow multiplier

; P is the pulses / L

; W is the width of the nozzle (mm)

; Z is the expected layer height

M756 T11 S1 ; set flow for the first layer

M674 T11 S2.0; turn on turbo mode

```
G54 X0 Y0 Z0 ; set offsets to zero
;***Print Lines***
M722 S10000 E5000 P1000 T11 I1 ; prime
; S is the rate (pulse per second)
; E is the number of pulses
; P is the pause before next command (ms)
G4 S.5 ; pause for .5 sec
M722 S10000 E300 P100 T11 ; reset to lower prime values
G0 X375 Y90 ; move to starting position
G1 Z1 F300 ; set layer height to 1mm
G1 X175 Y90 F300 E1 ; print starter line
G1 X175 Y100 F300 E1 ; jog down
G1 X375 Y100 F300 E1 ; complete first line
G1 X375 Y110 F300 E1 ; jog down
G1 X175 Y110 F300 E1 ; print second line
G1 X175 Y120 F300 E1 ; jog down
G1 X375 Y120 F300 E1 ; print third line
G1 X375 Y130 F300 E1 ; jog down
G1 X175 Y130 F300 E1 ; print fourth line
G1 X175 Y140 F300 E1 ; jog down
G1 X375 Y140 F300 E1 ; print fifth line
G0 Z10 ; move head up
G0 Z50 X500 ; move head out of way
M721 S10000 E5000 P500 T11 I1 ; unprime 5000 steps
G4 S.5 ; pause for unprime
M0 ; pause to put cap on to prevent excess material extrusion
;***Cure Lines***
```

```
T2 ; switch head to UV light pen
G1 Z9 E1 F1800 ; set working distance for cure
G54 X-70 Y25 Z9 ; set offset
M106 S100 T13 ; turn on light at 100% (S100)
G0 X375 Y90 Z1 ; go to starting position at 10mm Z
G1 X175 Y90 F300 E1 ; cure starter line
G1 X175 Y100 F300 E1 ; jog down
G1 X375 Y100 F300 E1 ; cure first line
G1 X375 Y110 F300 E1 ; jog down
G1 X175 Y110 F300 E1 ; cure second line
G1 X175 Y120 F300 E1 ; jog down
G1 X375 Y120 F300 E1 ; cure third line
G1 X375 Y130 F300 E1 ; jog down
G1 X175 Y130 F300 E1 ; cure fourth line
G1 X175 Y140 F300 E1 ; jog down
G1 X375 Y140 F300 E1 ; cure fifth line
M106 S0 T13 ; turn off UV light
T0 ; switch back to first head
G53 ; clear offsets
G0 X0 Y0 ; go home
M30 ; end program
```

Minimalist Line Test GCode (No Commented Code)

```
M203 X8000 Y8000 Z1000
G21
G90
G53
```

G28 X0 Y0

M221 T11 S1 P30 W1.6 Z1

M756 T11 S1

M674 T11 S2.0

G54 X0 Y0 Z0

M722 S10000 E5000 P1000 T11 I1

G4 S.5

M722 S10000 E300 P100 T11

G0 X375 Y90

G1 Z1 F300

G1 X175 Y90 F300 E1

G1 X175 Y100 F300 E1

G1 X375 Y100 F300 E1

G1 X375 Y110 F300 E1

G1 X175 Y110 F300 E1

G1 X175 Y120 F300 E1

G1 X375 Y120 F300 E1

G1 X375 Y130 F300 E1

G1 X175 Y130 F300 E1

G1 X175 Y140 F300 E1

G1 X375 Y140 F300 E1

G0 Z10

G0 Z50 X500

M721 S10000 E5000 P500 T11 I1

G4 S.5

M0

T2

```
G1 Z9 E1 F1800
G54 X-70 Y25 Z9
M106 S100 T13
G0 X375 Y90 Z1
G1 X175 Y90 F300 E1
G1 X175 Y100 F300 E1
G1 X375 Y100 F300 E1
G1 X375 Y110 F300 E1
G1 X175 Y110 F300 E1
G1 X175 Y120 F300 E1
G1 X375 Y120 F300 E1
G1 X375 Y130 F300 E1
G1 X175 Y130 F300 E1
G1 X175 Y140 F300 E1
G1 X375 Y140 F300 E1
M106 S0 T13
T0
G53
G0 X0 Y0
M30
```

NOTE: This code is compatible with the Repetrel software as of April 2019. Due to frequent software updates and new versions, alterations may need to be made to accommodate printers at other institutions.

REFERENCES

[1] C. W. Hull, "The Birth of 3D Printing," *Research-Technology Management*, vol. 58, pp. 25–30, 6 2015.

[2] A. Khalyfa, S. Vogt, J. Weisser, G. Grimm, A. Rechtenbach, W. Meyer, and M. Schnabelrauch, "Development of a new calcium phosphate powder-binder system for the 3D printing of patient specific implants," *Journal of Materials Science: Materials in Medicine*, vol. 18, pp. 909–916, 5 2007.

[3] R. Liu, Z. Wang, T. Sparks, F. Liou, and J. Newkirk, *Laser Additive Manufacturing: Materials, Design, Technologies, and Applications*. Woodhead Publishing, 2017.

[4] T. Guo, T. R. Holzberg, C. G. Lim, F. Gao, A. Gargava, J. E. Trachtenberg, A. G. Mikos, and J. P. Fisher, "3D printing PLGA: a quantitative examination of the effects of polymer composition and printing parameters on print resolution," *Biofabrication*, vol. 9, p. 024 101, 2017.

[5] E. Ozkol, W. Zhang, J. Ebert, and R. Telle, "Potentials of the Direct inkjet printing method for manufacturing 3Y-TZP based dental restorations," *Journal of the European Ceramic Society*, vol. 32, pp. 2193–2201, 10 2012.

[6] A. Dawood, B. M. Marti, V. Sauret-Jackson, and A. Darwood, "3D printing in dentistry," *BDJ*, vol. 219, pp. 521–529, 2015.

[7] Q. Liu, M. C. Leu, and S. M. Schmitt, "Rapid prototyping in dentistry: Technology and application," *Int J Adv Manuf Technol*, vol. 29, pp. 317–335, 2006.

[8] J. Zhang and Y.-G. Jung, *Additive Manufacturing: Materials, Processes, Quantifications and Applications*. Butterworth-Heinemann, 2018.

[9] M. Savastano, C. Amendola, F. DAscenzo, and E. Massaroni, "3-D Printing in the Spare Parts Supply Chain: An Explorative Study in the Automotive Industry," *Digitally Supported Innovation Lecture Notes in Information Systems and Organisation*, vol. 18, 2016.

[10] L. N. Marcincinova and I. Kuric, "Basic and advanced materials for fused deposition modeling rapid prototyping technology," *Manuf. and Ind. Eng*, vol. 11, pp. 2193–2204, 1 2012.

[11] P. F. Jacobs, *Rapid Prototyping and Manufacturing Fundamentals of Stereolithography*. Society of Manufacturing Engineers, 1992.

[12] J. J. Beaman and C. R. Deckard, *Selective laser sintering with assisted powder handling*, US Patent 4,938,816, 1990.

[13] J. P. Kruth, P. Mercelis, J. V. Vaerenbergh, L. Froyen, and M. Rombouts, "Binding mechanisms in selective laser sintering and selective laser melting," *Rapid Prototyping Journal*, vol. 11, pp. 26–36, 1 2005.

[14] N. Travitzky, A. Bonet, B. Dermeik, T. Fey, I. Filbert-Demut, L. Schiler, T. Schlordt, and P. Greil, "Additive manufacturing of ceramic-based materials," *Advanced Engineering Materials*, vol. 16, pp. 729–754, 6 2014.

[15] J. A. Lewis and G. M. Gratson, "Direct writing in three dimensions," *Materials Today*, vol. 7, pp. 32–39, 2004.

[16] Z. Ozdemir, E. Hernandez-Nava, A. Tyasa, J. A. Warren, S. D.Fay, R. Goodall, Iain-Todd, and H. Askes, "Energy absorption in lattice structures in dynamics experiments," *International Journal of Impact Engineering*, vol. 89, pp. 49–61, 2016.

[17] J. A. Lewis, "Direct Ink Writing of 3D Functional Materials," *Advanced Functional Materials*, vol. 16, pp. 2193–2204, 2006.

[18] L. Rueschhoff, W. Costakis, M. Michie, J. Youngblood, and R. Trice, "Additive manufacturing of dense ceramic parts via direct ink writing of aqueous alumina suspensions," *Int. J. Appl. Ceram. Technol*, vol. 13, pp. 821–830, 5 2016.

[19] J. A. Lewis, "Direct-write assembly of ceramics from colloidal inks," *Current Opinion in Solid State and Materials Science*, vol. 6, pp. 245–250, 2002.

[20] M. Sweeney, L. L. Campbell, J. Hanson, M. L. Pantoya, and G. F. Christopher, "Characterizing the feasibility of processing wet granular materials to improve rheology for 3D printing," *J Mater Sci*, vol. 52, pp. 13 040–13 053, 2017.

[21] M. M. Rueda, M.-C. Auscher, R. Fulchiron, T. Périé, G. Martin, P. Sonntag, and P. Cassagnau, "Rheology and applications of highly filled polymers a review of current understanding," *Progress in Polymer Science*, vol. 66, pp. 22–53, 2017.

[22] J. Mewis and N. J. Wagner, *Colloidal Suspension Rheology*. Cambridge University Press, 2012.

[23] R. Schwarze, A. Gladkyy, F. Uhlig, and S. Luding, "Rheology of weakly wetted granular materials: A comparison of experimental and numerical data," *Granular Matter*, vol. 15, pp. 455–465, 4 2013.

[24] T. Durig and K. Karan, *Handbook of Pharmaceutical Wet Granulation, Chapter 9 Binders in Wet Granulation*. Elsevier, 2019.

[25] H. A. Barnes, *A Handbook of Elementary Rheology*. University of Wales, Institute of Non-Newtonian Fluid Mechanics, 2000.

[26] D. M. Kalyon and S. Aktas, "Factors affecting the rheology and processability of highly filled suspensions," *Annual Review of Chemical and Biomolecular Engineering*, vol. 5, pp. 229–254, 2014.

[27] C. Partkinson, S. Matsumoto, and P. Sherman, "The influence of particle-size distribution on the apparent viscosity of non-newtonian dispersed systems," *Journal of Colloid and Interface Science*, vol. 33, pp. 150–160, 1 1970.

[28] B. J. Konijn, O. B. J. Sanderink, and N. P. Kruyt, "Experimental study of the viscosity of suspensions: Effect of solid fraction, particle size and suspending liquid," *Powder Technology*, vol. 266, pp. 61–69, 2014.

[29] T. Tadros, "Interparticle interactions in concentrated suspensions and their bulk (rheological) properties," *Advances in Colloid and Interface Science*, vol. 168, pp. 263–277, 1–2 2011.

[30] S. Torquato, T. M. Truskett, and P. G. Debenedetti, "Is random close packing of spheres well defined," *Physical Review Letters*, vol. 84, pp. 2064–2067, 10 2000.

[31] A. Guyot, F. Chu, M. Schneider, C. Graillat, and T. McKenna, "High solid content latexes," *Progress in Polymer Science*, vol. 27, pp. 1573–1615, 2002.

[32] C. Servais, R. Jones, and I. Roberts, "The influence of particle size distribution on the processing of food," *Journal of Food Engineering*, vol. 51, pp. 201–208, 2002.

[33] H. J. H. Brouwers, "Particle-size distribution and packing fraction of geometric random packings," *Physical Review E*, vol. 74, pp. 2064–2067, 10 2006.

[34] K. To, P.-Y. Lai, and H. K. Pak, "Jamming of granular flow in a two-dimensional hopper," *PHYSICAL REVIEW LETTERS*, vol. 86, 1 2001.

[35] E. Brown, "Dynamic jamming point for shear thickening suspensions," *Physical Review Letters*, vol. 103, pp. 213–245, 086001 2000.

[36] M. E. Cates, J. P. Wittmer, J. P. Bouchaud, and P. Claudin, "Jamming and static stress transmission in granular materials," *Chaos: An Interdisciplimary Journal of Nonlinear Science*, vol. 9, pp. 511–522, 3 1999.

[37] F. Radjai, S. Roux, and J. J. Moreau, "Contact forces in a granular packing," *Chaos*, vol. 9, pp. 544–550, 3 1999.

[38] M. E. Cates, J. P. Wittmer, J. P. Bouchaud, and P. Claudin, "Jamming, force chains, and fragile matter," *Physical Review Letters*, vol. 81, pp. 1841–1844, 9 1998.

[39] E. Brown and H. M. Jaeger, "Shear thickening in concentrated suspensions: Phenomenology, mechanisms, and relations to jamming," *Reports on Progress in Physics*, vol. 77, 4 2014.

[40] D. Bi, J. Zhang, B. Chakraborty, and R. P. Behringer, "Jamming by shear," *Nature*, vol. 480, pp. 355–358, 2011.

[41] S. S. Samudre, U. R. Nair, G. M. Gore, R. K. Sinha, A. K. Sikder, and S. N. Asthana, "Studies on an Improved Plastic Bonded Explosive (PBX) for Shaped Charges," *Propellants Explosives and Pyrotechnics*, vol. 34, pp. 145–150, 2009.

[42] M.B.Talawar, S.K.Jangid, T.Nath, R.K.Sinha, and S.N.Asthana, "New directions in the science and technology of advanced sheet explosive formulations and the key energetic materials used in the processing of sheet explosives: Emerging trends," *Journal of Hazardous Materials*, vol. 300, pp. 307–321, 2015.

[43] B. R.Clark, M. L.Pantoya, E. M.Hunt, T. J.Kelly, B. F.Allen, R. J.Heaps, and M. A.Daniels, "Synthesis and characterization of flexible, free-standing, energetic thin films," *Journal of Hazardous Materials*, vol. 284, pp. 422–426, 2015.

[44] C. M. Tarver, "Critical conditions for impact- and sock-induced hot spots in solid explosives," *Journal of Physical Chemistry*, vol. 100, pp. 5794–5799, 1996.

[45] A. Barua, S. Kim, Y. Horie, and M. Zhou, "Prediction of probabilistic ignition behavior of polymer-bonded explosives from microstructural stochasticity," *Journal of Applied Physics*, vol. 113, p. 184 907, 2013.

[46] A. Barua, S. Kim, and M. Zhou, "Ignition criterion for heterogeneous energetic materials based on hotspot size-temperature threshold," *Journal of Applied Physics*, vol. 113, p. 064 906, 2013.

[47] A. Barua and M. Zhou, "A Lagrangian Framework for Analyzing Microstructural Level Response of Polymer-Bonded Explosives," *Modelling and Simulation in Materials Science and Engineering*, vol. 19, p. 055 001, 2011.

[48] M. A. Daniel, "Polyurethane binder systems for polymer bonded explosives," 2006.

[49] D. R. Drodge and D. M. Williamson, "Understanding damage in polymer-bonded explosive composites," *Journal of Materials Science*, vol. 51, pp. 668–679, 2 2016.

[50] D. Wang, B. Zheng, C. Guo, B. Gao, J. Wang, G. Yang, H. Huang, and F. Nie, "Formulation and performance of functional sub-micro CL-20-based energetic poly-

mer composite ink for direct-write assembly," *RSC Advances*, vol. 6, pp. 112 325–112 331, 113 2016.

[51] A. Elbeih, "Effect of different polymeric matrices on some properties of plastic bonded explosives," *Propellants Explosives and Pyrotechnics*, vol. 37, pp. 676–684, 2012.

[52] F. D. Ruz-Nuglo, L. J. Groven, and J. A. Puszynski, "Additive manufacturing for energetic components and materials," *AIAA Propulsion and Energy Forums*, vol. 66, pp. 22–53, 2014.

[53] K. J. Ramos, B. J. Jensen, A. J. Iverson, J. D. Yeager, C. A. Carlson, D. S. Montgomery, D. G. Thompson, K. Fezzaa, and D. E. Hooks, "In situ investigation of the dynamic response of energetic materials using impulse at the advanced photon source," *Journal of Physics: Conference Series*, vol. 500, p. 142 028, 2014.

[54] Z. Zhou, P. Chen, Z. Duan, and F. Huang, "Study on fracture behavior of a polymer-bonded explosive simulant subjected to uniaxial compression using digital image correlation method," *Strain*, vol. 48, pp. 326–332, 2012.

[55] J. Corley, W. Riedel, S. Hiermaier, P. Weidemaier, and K. Thoma, "A combined experimental/computational approach for assessing the high strain rate response of high explosive simulants and other viscoelastic particulate composite materials," *AIP Conference Proceedings*, vol. 620, 705 2002.

[56] M. Rubinstein and R. H. Colby, *Polymer Physics*. Oxford University Press, 2003.

[57] R. J. Young and P. A. Lovell, *Introduction to Polymers*. CRC Press Taylor and Francis Group, 2011.

[58] A. E. Jakus, S. L. Taylor, N. R. Geisendorfer, D. C. Dunand, and R. N. Shah, "Metallic Architectures from 3D-Printed Powder-Based Liquid Inks," *Adv. Funct. Mater.*, 2015.

[59] J. W. Halloran, "Ceramic stereolithography: Additive manufacturing ceramics by photopolymerization," *Annual Review of Materials Research*, vol. 46, pp. 19–40, 2016.

[60] Z. Tonglai, H. Rongzu, X. Yi, and L. Fuping, "Jamming of granular flow in a two-dimensional hopper," *Thermochimica Acta*, vol. 244, pp. 171–176, 1994.

[61] P. Weiss, "Photo-induced polymerization," *Pure and Applied Chemistry*, vol. 15, pp. 587–600, 1967.

[62] E. W. Nelson, T. P. Carter, and A. B. Scranton, "Fluorescence monitoring of cationic photopolymerizations: Divinyl ether polymerizations photosensitized by anthracene derivatives," *Macromolecules*, vol. 27, pp. 1013–1019, 4 1994.

[63] M. A. Tehfe, F. Louradour, J. Laleve, and J.-P. Fouassier, "Photopolymerization reactions: On the way to a green and sustainable chemistry," *Appl. Sci.*, vol. 3, pp. 490–514, 2 2013.

[64] Y. Guo, Z. Ji, Y. Zhang, X. Wang, and F. Zhou, "Solvent-free and photocurable polyimide inks for 3D printing," *Journal of Materials Chemistry A*, vol. 5, pp. 16 307–16 314, 2017.

[65] J. L. Ferracane, "Developing a more complete understanding of stresses produced in dental composites during polymerization," *Dental Materials*, vol. 21, pp. 36–42, 2005.

[66] L. C. Nicolae, "The Effect of UDMA/TEGDMA Mixtures and Bioglass Incorporation on the Mechanical and Physical Properties of Resin and Resin-Based Composite Materials," *Conference Papers in Science*, vol. 2014, 2013.

[67] P. K. Shah and J. W. Stansbury, "Role of filler and functional group conversion in the evolution of properties in polymeric dental restoratives," *Dental Materials*, vol. 30, pp. 586–593, 2014.

[68] J.-D. Cho, "Photocuring Kinetics of UV-Initiated Free-Radical Photopolymerizations with and without Silica Nanoparticles," *Journal of Polymer Science: Part A: Polymer Chemistry*, vol. 43, pp. 658–670, 2005.

[69] N. Moszner and U. Salz, "New developments of polymeric dental composites," *Progress in Polymer Science*, vol. 26, pp. 535–576, 2001.

[70] F. Gonçalves, Y. Kawano, and R. R. Braga, "Contraction stress related to composite inorganic content," *Dental Materials*, vol. 26, pp. 704–709, 7 2010.

[71] H. A. Sunbul, N. Silikas, and D. C. Watts, "Polymerization shrinkage kinetics and shrinkage-stress in dental resin-composites," *Dental Materials*, vol. 32, pp. 998–1006, 2016.

[72] M. Pilkenton, J. Lewman, and R. Chartoff, "Effect of oxygen on the crosslinking and mechanical properties of a thermoset formed by free-radical photocuring," *Journal of Applied Polymer Science*, 2010.

[73] C. Charton, V. Falk, P. Marchal, F. Pla, and P. Colon, "Influence of Tg, viscosity and chemical structure of monomers on shrinkage stress in light-cured dimethacrylate-based dental resins," *Dental Materials*, vol. 23, pp. 1447–1459, 2007.

[74] Ciba, "IRGACURE 184 Photoinitiator," *http://www.xtgchem.cn/upload/20110629045332.PDF*, pp. 22–53, 2001.

[75] M. T. Shaw, "On Estimating The Zero-Shear-Rate Viscosity Tests With PIB And PDMS," *Annual Review of Chemical and Biomolecular Engineering*, vol. 5, pp. 229–254, 2014.

[76] MalvernPanalytical, *Mastersizer 3000: Smarter particle sizing*, https://www.malvernpanalytical.com range/mastersizer-range/mastersizer-3000, 2019.

[77] M. Panalytical, *A basic guide to particle characterization*, 2015.

[78] FlackTekInc, *Speedmixer technology*, https://speedmixer.com/speedmixer-technology/, 2019.

[79] D. M. Kaylon, "An overview of the rheological behavior and characterization of energetic formulations: Ramifications on safety and product quality," *Journal of Energetic Materials*, vol. 24, pp. 213–245, 2006.

[80] V. Vand, "Viscosity of solutions and suspensions. i. theory," *Journal of Physical Chemistry*, vol. 52, pp. 277–299, 1948.